OXFORD

Journal of Petrology, 2025, **66**, egaf054
https://doi.org/10.1093/petrology/egaf054
ADVANCE ACCESS PUBLICATION DATE 29 MAY 2025
Original Manuscript

Mush Disaggregation and Dike Propagation Timescales at Active Volcanoes: Evidence from the 2022–2023 Fagradalsfjall Eruptions

ALBERTO CARACCIOLO[1,2,*], EDWARD W. MARSHALL[1,3], EUAN J. F. MUTCH[4], ENIKŐ BALI[1], SÆMUNDUR A. HALLDÓRSSON[1], SIMON MATTHEWS[1], OLGEIR SIGMARSSON[1,5], JOHN MACLENNAN[6], HEINI MERRILL[1], BRYNDÍS ÝR GISLADÓTTIR[1], SÓLEY JOHNSON[1], MAREN KAHL[7], GUðMUNDUR H. GUðFINNSSON[1], JÓHANN GUNNARSSON ROBIN[1] and REBEKKA H. RÚNARSDÓTTIR[1]

[1]Nordic Volcanological Centre, Institute of Earth Sciences, University of Iceland, Sturlugata 7, 102, Reykjavík, Iceland
[2]Department of Physics and Geology, University of Perugia, Piazza Università, 06123, Perugia, Italy
[3]GeoZentrum Nordbayern, Friedrich-Alexander University Erlangen-Nuremburg, Schlossgarten 5, 91054, Erlangen-Nuremburg, Germany
[4]Earth Observatory of Singapore, Nanyang Technological University, 50 Nanyang Ave, 639798, Singapore, Singapore
[5]Laboratoire Magmas et Volcans, Université Clermont Auvergne, 6 Av. Blaise Pascal, 63170, Aubière, France.
[6]Department of Earth Sciences, University of Cambridge, Downing St, CB2 3EQ, Cambridge, UK
[7]Ruhr-Universität Bochum, Institute for Geology, Mineralogy and Geophysics, Universitätsstraße 150, 44801, Bochum, Germany

*Corresponding author. E-mail: alberto@hi.is

The architectures of magma plumbing systems and timescales of magmatic processes are fundamental to understanding volcanic eruption dynamics. This is especially crucial when investigating the rejuvenation of magma plumbing system that have been dormant for extended periods, as their long-term evolution is poorly understood, making eruption monitoring more challenging. The 2021–2023 Fagradalsfjall eruptions provide a unique perspective on the initial stages and temporal evolution of a basaltic magma plumbing system, since its previous eruptions occurred ∼7000 years ago. In this study, we focus on the 2022 and 2023 Fagradalsfjall eruptions, integrating our petrological and geochemical dataset with data from the 2021 Fagradalsfjall eruption. We show that the 2022 and 2023 Fagradalsfjall eruptions were sourced from a near-Moho magma domain at ∼14 km depth, similar to the 2021 Fagradalsfjall eruption. However, clinopyroxene–melt barometry suggests that the 2022 and 2023 magmas experienced crystallization in an incipient mid-crustal reservoir or during slow ascent within the magma conduit. The 2022 and 2023 Fagradalsfjall lavas show substantially less compositional variation than the 2021 lavas and are dominated by geochemically enriched compositions that became apparent after the first 40 days of the 2021 event. Olivine mesocrysts (100–500 μm in length) and plagioclase macrocrysts (>500 μm in length) constitute two different populations in the crystal cargo. Olivine mesocrysts are interpreted as autocrysts that crystallized from the host magma, whereas the plagioclase crystals, which are out of chemical equilibrium with the host magma, are derived from a crystal mush. Olivine and plagioclase diffusion timescales represent two different processes. Plagioclase diffusion timescales reveal the erosion of crystal mushes, a process that unfolded over the months and days prior to the 2022 and 2023 eruptions. The decreasing duration of these timescales from 2021 to 2023 suggests an increasingly rapid response of the plumbing system to deep melt injections and the progressive shortening of unrest timescales. In contrast, olivine diffusion timescales capture the timing and duration of dike opening and propagation from near-Moho depths, as evidenced by the correlation between their cumulative frequency distribution and pre-seismic activity. Combined geophysical, petrological, and barometric data suggest that the 2022–2023 propagating dikes took significantly longer to traverse the lower crust and reach mid-crustal levels compared to the upper crust, which they breached within a few days through a fully established magma pathway. Our results highlight the importance of deep magmatic processes and the need to improve monitoring methods for detecting the early stages of magma accumulation and dike propagation at active volcanoes in geological settings similar to Iceland.

Key words: Geothermobarometry; Basaltic magma; Diffusion modelling; Iceland; Fagradalsfjall eruption; Petrological monitoring

INTRODUCTION

Volcanic eruptions are the result of a complex interplay of magmatic processes, including the accumulation, storage, transport, and evolution of magma. These processes take place within the magma plumbing system—a complex network of interconnected sills, mushes and dikes that regulate magma processing (Cashman *et al.*, 2017; Magee *et al.*, 2018; Maclennan, 2019). Notably, the structure of magma plumbing systems and the timescales of magmatic processes can evolve over time, with several studies highlighting changes occurring on both long (centuries to millennia) (Mutch *et al.*, 2019a; Caracciolo *et al.*, 2020, 2021; Lo Forte *et al.*, 2023) and short timescales (days to years) (Kahl *et al.*, 2015; Mutch *et al.*, 2019b; Davydova *et al.*, 2022; Halldórsson *et al.*, 2022; Marshall *et al.*, 2024; Matthews *et al.*, 2024).

The Reykjanes Peninsula (RP), in southwest Iceland, provides a unique opportunity to study the temporal evolution of magma plumbing systems, as it has been experiencing volcano-tectonic unrest since December 2019 (Cubuk-Sabuncu *et al.*, 2021; Flóvenz *et al.*, 2022; Sigmundsson *et al.*, 2022, 2024; Einarsson *et al.*, 2023;

RECEIVED DECEMBER 17, 2024; **REVISED** APRIL 8, 2025; **ACCEPTED** MAY 25, 2025

Jenkins et al., 2025; Parks et al., 2025), the first in the area since the medieval period (Fig. 1; Sæmundsson et al. (2020). In particular, the Fagradalsfjall volcanic system, dormant for the past ~7000 years (Einarsson et al., 2023), has erupted three times since 2021, offering a rare opportunity to investigate the rejuvenation of a basaltic magma plumbing system and the short-term evolution of magmatic processes. For example, these eruptions allow us to test whether the plumbing system undergoes significant changes in magma composition, P–T–X–fO_2 storage conditions, and transport processes, as observed during the 2021 eruption (Halldórsson et al., 2022; Pedersen et al., 2022; Marshall et al., 2024), or if it rapidly transitions into a more established and stable plumbing system. Furthermore, observations from the geological record in the RP indicate that once volcanic unrest begins, it may persist for decades or even centuries (Sæmundsson et al., 2020). This highlights the importance of understanding temporal changes in the magma plumbing system to support hazard mitigation strategies. So far, significant research has focused on the initial eruption of this series, the 2021 Fagradalsfjall eruption (Lamb et al., 2021; Bindeman et al., 2022; Greenfield et al., 2022; Halldórsson et al., 2022; Sigmundsson et al., 2022; Hjartardóttir et al., 2023; Kahl et al., 2023; Scott et al., 2023; Day et al., 2024; Marshall et al., 2024; Soubestre et al., 2025), which was subsequently followed by two additional eruptions at Fagradalsfjall: one at Meradalir in 2022 and another at Litli-Hrútur in 2023 (Fig. 1).

Previous studies of the 6-month-long 2021 Fagradalsfjall eruption highlight that it differed significantly from most basaltic eruptions globally (Halldórsson et al., 2022). The 2021 eruption was fed from a magma domain (hereafter defined as a single or a set of interconnected magma reservoirs) located at near-Moho depths (Halldórsson et al., 2022; Marshall et al., 2024; Jenkins et al., 2025), rather than at mid-crustal depths like most Icelandic eruptions (Neave & Putirka, 2017; Caracciolo et al., 2020, 2023; Baxter et al., 2023). Remarkable changes in incompatible minor and trace element ratios, as well as radiogenic isotopes, were observed (Halldórsson et al., 2022) throughout the eruption, again, unlike most Icelandic eruptions which typically display invariant lava compositions throughout the eruption (Sigmarsson et al., 1991; Halldórsson et al., 2018). The geochemical variability of the 2021 Fagradalsfjall eruption can be attributed to the contribution of multiple sills, located in the lower crust and near the crust–mantle boundary (Marshall et al., 2024). While each sill may host a chemically uniform melt, the erupted composition may vary over time as the supply from each chemically distinct sill waxes and wanes (Marshall et al., 2024). Based on diffusion chronometry, the deep magmatic unrest recorded in the 2021 crystal cargo began years before the eruption, while magma started to move and traverse the crust without noticeable petrological record of mid-crustal re-equilibration in the months and days prior to the eruption (Kahl et al., 2023).

In this work, we study the geochemistry and petrology of the 2022 and 2023 Fagradalsfjall eruptions in order to explore the temporal variations within the magma plumbing system in the earliest stages of 'reawakening' after thousands of years of dormancy. We present major element analyses of glass and minerals, along with trace element data and Sr-Nd-Hf-Pb isotopes from a time-series of samples collected during the 2022 and 2023 Fagradalsfjall eruptions. Additionally, we report diffusion timescale data for olivine and plagioclase crystals erupted in 2022 and 2023, linking these findings to monitoring signals and petrological constraints (e.g. Kahl et al., 2023; Parks et al., 2023). Combined with previous work from the 2021 eruption, our results provide a window into the escalation of volcanic unrest and the timescales of dike propagation from near-Moho depths, with potential implications for the progression of volcanic hazards at other localities across the Reykjanes Peninsula and rift eruptions globally.

GEOLOGICAL BACKGROUND

Geological setting and events leading to the eruptions

Located in southwest Iceland, the RP has been an active oblique spreading zone for approximately 6–7 million years (Einarsson, 2008). It features five distinct volcanic systems, listed west to east: Reykjanes, Svartsengi, Fagradalsfjall, Krýsuvík, and Brennisteinsfjöll (Fig. 1A; Einarsson et al. (2023). Studies of past eruptions on the RP reveal that eruptive periods occur cyclically, each cycle lasting approximately 1000 years and the eruptive period a few hundred years, with the last occurring between 800 and 1240 AD (Sæmundsson et al., 2020). Volcanic activity on the RP recommenced in 2021 with the Fagradalsfjall eruption, consistent with the cyclic nature of eruptions observed in this region (Sæmundsson et al., 2020).

Since mid-December 2019, episodes of intense seismic activity related to magmatic intrusions and triggered earthquakes have marked the onset of tectonic unrest across the RP (Sigmundsson et al., 2022). In 2020, three inflation episodes occurred in Reykjanes, Svartsengi, and Krýsuvík (Sigmundsson et al., 2022; Parks et al., 2025), possibly related to deep magma migration (Parks et al., 2025) or a combination of magma and supercritical magmatic fluids (Flóvenz et al., 2022). On February 24, 2021, a magnitude 5.6 earthquake initiated increased seismic activity at Fagradalsfjall. Subsequently, a NE–SW striking dike began propagating, as indicated by ground deformation. About 3 weeks later, on March 19, this dike reached the surface, marking the onset of the 2021 eruption in Geldingadalir valley at Fagradalsfjall (Barsotti et al., 2022; Greenfield et al., 2022; Sigmundsson et al., 2022; Einarsson et al., 2023). The eruption continued for ~6 months (183 days), until September 18, 2021, extruding a bulk volume of $\sim 150 \times 10^6$ m^3 (Fig. 1B; (Pedersen et al., 2022). The 2021 eruption was characterized by a fairly constant effusion rate from March to September, except for a sudden increase in May (Pedersen et al., 2022). Following the 2021 eruption, a second dike intrusion occurred at Fagradalsfjall in December 2021, which did not culminate in an eruption. In April 2022, the fourth inflation episode (inflation IV) in the RP was recorded in Svartsengi (Parks et al., 2023, 2025). Eventually, after ~10 months of quiescence, a third dike began propagating in Fagradalsfjall on July 30, 2022, erupting on the surface four days later along a ~230 m long fissure in the Meradalir valley, 1.5 km NE of the 2021 eruptive craters (Fig. 1C; (Gunnarson et al., 2023; Parks et al., 2023, 2025; Pedersen et al., 2024). The 2022 eruption lasted for ~18 days and extruded a bulk volume of $\sim 11 \times 10^6$ m^3 of lava (Gunnarson et al., 2023; Pedersen et al., 2024). From the end of the 2022 eruption and before the start of the 2023 eruption, only subtle inflation was measured, with increased inflation rates measured at Svartsengi in the month before the 2023 eruption (inflation V) (Parks et al., 2025). Eventually, a fourth dike began propagating at Fagradalsfjall on July 3, 2023. This dike erupted on July 10, 2023, across a ~220 m long fissure at the bottom of the Litli-Hrútur hill, ~3 km NE of the 2022 eruptive craters. The 2023 eruption lasted for 26 days and the bulk erupted volume was $\sim 15 \times 10^6$ m^3 (Fig. 1D; Belart et al., 2023; Pedersen et al., 2024). In contrast to the 2021 eruption, the effusion rate exponentially declined over the course of both 2022 and 2023 eruptions (Pedersen et al., 2024). Following the 2023 eruption at Fagradalsfjall, seismicity increased dramatically in the Svartsengi

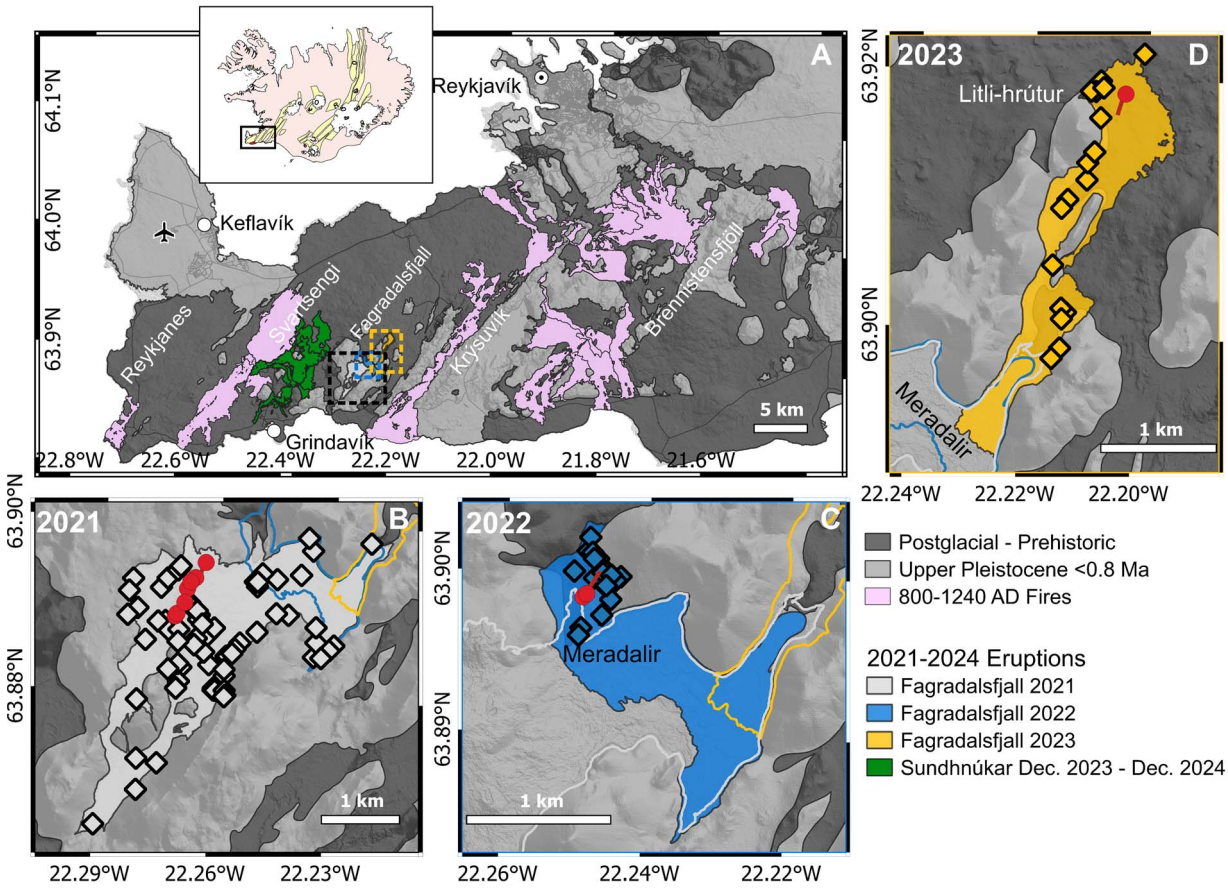

Fig. 1. (**A**) Simplified geological map of the Reykjanes Peninsula, showing the background geology and the location of the different volcanic systems (Sæmundsson *et al.*, 2016). Highlighted on the map is the aerial extent of lavas erupted during the medieval period (800–1240 AD Fires) across the Reykjanes Peninsula, as well as the lavas erupted from 2021 to 2024 in Fagradalsfjall and Svartsengi. The extents of the lavas erupted in Svartsengi between December 2023 and November 2024 are sourced from Landmælingar Íslands Geoserver (gis.lmi.is/geoserver). Urban areas are indicated with dashed black outlines. (**B**–**D**) Sample locality maps and aerial extents of the (**B**) 2021, (**C**) 2022 and (**D**) 2023 Fagradalsfjall lava fields. Samples from the 2021 eruption are from Halldórsson *et al.* (2022) and Marshall *et al.* (2024). Sample localities are shown with diamonds and coloured according to the eruption. This colour-coding is maintained throughout the manuscript. Red solid lines show the location of the eruptive fissure, while filled red circles indicate the different vents that opened during the eruptions. The lava fields from the 2021, 2022, and 2023 eruptions are from Pedersen *et al.* (2022), Gunnarson *et al.* (2023) and Belart *et al.* (2023), respectively.

area in October 2023, followed by several inflation episodes near the town of Grindavík. These episodes led to the formation of ten dikes and eight relatively short-lived eruptions (lasting hours to weeks) between November 2023 and April 2025 (Matthews *et al.*, 2024; Sigmundsson *et al.*, 2024; Parks *et al.*, 2025). In this study, we focus on products from the 2022 eruption at Meradalir and the 2023 eruption at Litli-Hrútur in the Fagradalsfjall volcanic system (Fig. 1).

SAMPLING

Throughout the eruptions, we frequently sampled freshly erupted materials. Our collection includes samples of quenched lava obtained by scooping molten lava into water-filled buckets, naturally cooled lava, and air-quenched tephra (Fig. 1). We assigned specific dates of vent emergence to naturally cooled and water-quenched lava samples by using field observations. Challenges in assigning a specific date of vent emergence include the short duration of the eruptions and the formation of a lava lake around the 2022 eruptive craters, where lava ponded before breaking out at the edge of the lava field. Therefore, when the eruption date could not be precisely determined, a range of dates was assigned to a sample. Tephra samples were collected from the ground when they could be linked to a specific time or period of vent emergence. Most tephra samples from the 2022 eruption were collected directly as they fell to the ground, still hot and requiring water-cooling before handling. Fewer tephra samples were obtained during the 2023 eruption due to unfavourable wind direction and strong moss fires caused by the lava at the beginning of the eruption, making it challenging to collect samples near the vent. A total of 19 samples from the 2022 eruption and 18 samples from the 2023 eruption are presented in this work and listed in Supplementary Table S1 (SDT1).

METHODS

Geochemical analytical methods

As in Marshall *et al.* (2024), we analysed the chemical composition of glass, minerals, whole-rock and macrocryst-free matrix. The latter reflects the bulk composition of the matrix (glass, microlites and mesocrysts) after the macrocrysts have been picked out. The compositions of glass and minerals were analysed using an electron microprobe (EMPA), while whole-rock and macrocryst-free matrix samples were analysed for major elements, trace elements, and radiogenic isotopes using inductively coupled

plasma optical emission spectroscopy (ICP-OES), inductively coupled plasma mass spectrometry (ICP-MS), and multi-collector ICP-MS (MC-ICP-MS), respectively.

Electron microprobe methods

Major and minor element concentrations in glasses (n = 323), plagioclases (n = 394), olivines (n = 334), and clinopyroxenes (n = 321) were analysed by electron microprobe using the JEOL JXA-8230 SuperProbe at the University of Iceland. The microprobe settings are identical to those described in Caracciolo *et al.* (2023), and more information are provided in the Supplementary Material. Accuracy and precision were assessed by repeat measurements on secondary standard materials (see SDT6-SDT9). The 2σ accuracy and precision on olivine Forsterite (Fo, $Fo = 100 \times Mg_{mol}/(Mg + Fe_{Tot})_{mol}$, clinopyroxene Mg# ($Mg\# = 100 \times Mg_{mol}/(Mg + Fe_{Tot})_{mol}$) and plagioclase Anorthite (An, $An = 100 \times Ca_{mol}/(Ca + Na + K)_{mol}$] as measured by secondary reference materials are all better than 2%.

For olivine diffusion modelling, concentration profiles were acquired perpendicular to crystal margins, with spacing 4 to 5 μm, using identical analytical settings to those described in Caracciolo *et al.* (2023). Based on repeated analyses of olivine secondary standards over 10 sessions, the 2σ precision and accuracy of olivine forsterite (Fo) measurements are approximately 0.3% (SDT10). The olivine Fo precision derived from secondary standard analyses is very similar to precision derived from EMPA counting statistics (i.e. Poisson distribution) errors for each analysis. For plagioclase diffusion, profiles were measured using the same analytical conditions to those reported in Mutch *et al.* (2021). Chemical profiles were analysed with spatial resolution that was typically 5 to 10 μm at the rim and 10 to 15 μm in the core. 2σ accuracy of An and Mg based on repeated analyses of secondary standard is 2% and 10%, respectively. 2σ precision of Mg in plagioclase based on repeated analyses of secondary standard is 17%. However, since the plagioclase secondary standard contains very little Mg compared to our samples, we calculated the precision of Mg based on EMPA counting statistics errors, which is ∼5% (Supplementary Table S11, SDT11).

Bulk major, trace element, and radiogenic isotope methods

The major element composition of whole-rock and macrocryst-free matrix was analysed by inductively coupled plasma optical emission spectroscopy (ICP-OES) using the ThermoFisher iCAP 7400 Duo instrument at the University of Iceland Plasma Center. Procedures for powder digestion and ICP-OES analysis are identical to those described in Marshall *et al.* (2024) and Matthews *et al.* (2024). More information is provided in the Supplementary Material. Based on replicates of basaltic reference materials BHVO-1, W-2, and BIR-1, 2σ precision for all elements, except for P, is less than 5% and most of the time < 3%. The 2σ precision of K_2O/TiO_2 for BHVO-1, which has comparable K_2O and TiO_2 concentration to our samples, is 3.2% (SDT2–SDT3).

Trace element concentrations of picked matrix were determined over two sessions on the ThermoFisher iCAP RQ Quadrupole Inductively Coupled Plasma Mass-Spectrometer (ICP-MS) at the University of Iceland Plasma Centre. For each sample, 50 mg of hand-picked macrocryst-free matrix was digested following the method described in Marshall *et al.* (2024) and Matthews *et al.* (2024). Further details on the ICP-MS method is provided in the Supplementary Material. Precision was assessed using BHVO-2 standard powder. Based on replicates of BHVO-2, 2σ reproducibility is <5% for all trace elements, except for Cs and Pb. La/Yb, La/Sm, and Dy/Yb are reproduced within 2.2%, 1.9%, and 1.5%, respectively (SDT4).

Sr, Nd, Hf, and Pb chemical separation and isotope analyses of picked matrix were performed at the University of Iceland Plasma Center using the Nu Plasma 1 multicollector ICP-MS. New MC-ICP-MS Sr and Nd isotope data (n = 7) were combined with and supplement the TIMS Sr and Nd isotope data from the same eruptions (n = 4), published in Matthews *et al.* (2024). We analysed Hf and Pb isotopes in eight samples from the eruptions (SDT5). Pb and Hf isotope analyses were carried out following the procedure described in Halldórsson *et al.* (2018) and Marshall *et al.* (2024). Further information on the methods used is provided in the Supplementary Material.

Thermobarometry

Magma storage pressures were estimated using both clinopyroxene–melt and Olivine–Plagioclase–Augite–Melt (OPAM) barometers. We employed the clinopyroxene–melt barometer of Neave & Putirka (2017) (SEE = ±1.4 kbar, i.e. ±4.9 km), implemented in Thermobar (Wieser *et al.*, 2022). Clinopyroxenes were paired with melt compositions from their respective eruptions, with 459 melt compositions from 2022 and 304 from 2023. Additionally, we also tested a clinopyroxene–melt matching scheme using a larger dataset of clinopyroxene and melt compositions from the 2021, 2022, and 2023 eruptions, where matching was tested regardless of the specific eruption (see Fig. S1). In the cpx–melt barometry calculations, clinopyroxene compositions from the 2022 (n = 188) and 2023 (n = 133) Fagradalsfjall samples were tested for equilibrium with melt compositions consisting of macrocryst-free matrix, glasses and melt inclusion compositions from the 2021–2023 Fagradalsfjall eruptions published by Halldórsson *et al.* (2022) and Caracciolo *et al.* (2024). Equilibrium filters and calculation parameters in Thermobar include: (1) Observed DiHd, EnFs, and CaTs component values within ±0.06, ±0.05 and ± 0.03 of predicted values, respectively (Neave *et al.*, 2019) (2) Kd $\frac{Fe-Mg}{Cpx-Liq}$ values within ±0.03 of equilibrium values calculated using Eq. 35 from Putirka (2008) (3) Exclusion of clinopyroxene compositions with Al (6O) < 0.11, to account for sector zoning (Neave & Putirka, 2017). (4) Melt $Fe^{3+}/Fe_T = 0.15$ (5) Melt $H_2O = 0.3$, in agreement with MI data from Halldórsson *et al.* (2022). In total, 106 and 62 clinopyroxene compositions were successfully matched with at least one equilibrium melt composition from the 2022 and 2023 Fagradalsfjall samples, respectively.

For OPAM barometry (SEE = 1.1 kbar, i.e. ±3.7 km), we used the calibration of Higgins and Stock (2024). We used 242 and 87 melt compositions from the 2022 and 2023 Fagradalsfjall samples, respectively, including tephra, quenched lava glass and macrocryst-free matrix compositions. In addition to petrographic observations, OPAM saturation was tested by using the statistical approach discussed in Baxter *et al.* (2023). Only melt compositions returning a probability of fit (Pf) above 0.8, in agreement with Baxter *et al.* (2023), were assumed to be three-phase saturated and used in this study. However, quenched lava glass compositions are unlikely to reflect magma storage pressures, as they are affected by microlite crystallization on the surface before water quenching, which affects OPAM pressure estimates (Caracciolo *et al.*, 2023). Pressures were converted into depths assuming an average crustal density of 3000 kg/m^3 (Darbyshire *et al.*, 2000; Baxter *et al.*, 2023).

Melt storage temperatures were estimated on macrocryst-free matrix and tephra glass compositions by using eq. 16 (SEE = ± 19°C) of Putirka (2008) and the OPAM thermometer (MAE = ± 10°C) by Baxter & Maclennan (2024).

Diffusion modelling

The diffusive relaxation of Fe–Mg zoning in olivine and Mg zoning in plagioclase crystals was modelled using the Diffusion Chronometry Finite Elements and Nested Sampling (DFENS) method outlined by Mutch *et al.* (2021). DFENS uses different types of prior distributions for different parameters. In both olivine and plagioclase modelling, a log uniform prior of 10^{-2} to 10^{4} days was used to encapsulate the possible range of timescales. Gaussian priors with 1σ uncertainties were used for intensive parameters such as temperature, oxygen fugacity, pressure, and activity of silica. For both olivine and plagioclase modelling, temperature was set with a prior of 1205 ± 20°C. Temperature was chosen by averaging multiple temperature estimates using the melt-only OPAM thermometer by Baxter & Maclennan (2024) applied to primitive (MgO > 8 wt%) tephra glass compositions from the 2022 and 2023 products. The temperature uncertainty was set as 2σ of the mean absolute error (MAE = 10°C) reported Baxter & Maclennan (2024). Other intensive parameters specific to olivine and plagioclase will be discussed below and in the Supplementary Material.

In total, we obtained 118 diffusion timescales from olivine (n = 53) and plagioclase (n = 57) crystals erupted during the 2022 and 2023 Fagradalsfjall eruptions (SDT12 and SDT13). The total number of independent olivine (n = 53) and plagioclase (n = 57) timescales is larger than the number of modelled olivine (n = 43) and plagioclase (n = 52) crystals, as in some crystals, we measured and analysed more than one analytical traverse (Fig. S3). Examples of best-fit models for olivine and plagioclase crystals are shown in Fig. S2, whereas all models are shown in Figs S25 and S26. The raw diffusion profiles can be found in SDT10–11.

Olivine diffusion modelling

The olivine DFENS modelling approach numerically solves Fick's second law (Crank, 1979) with a spatially dependent diffusion coefficient. For Fe–Mg interdiffusion we use the diffusion coefficient parameterization and covariance matrix of Mutch *et al.*, (2019b) which is based on the diffusion coefficient data of Chakraborty (1997), Petry *et al.* (2004), Dohmen & Chakraborty (2007), Dohmen *et al.* (2007), Holzapfel *et al.* (2007) and Spandler & O'Neill (2010). Refer to Mutch *et al.* (2021) for more details of how the diffusion coefficient was set.

We obtained Fe–Mg timescales from 34 and 19 analytical traverses in 25 and 18 olivine crystals from the 2022 and 2023 Fagradalsfjall eruptions, respectively. Olivine crystals were modelled using a pressure prior of 1.7 ± 1.4 kbar, consistent with cpx–melt barometry constraints (Fig. S4). A Fe^{3+}/Fe_T prior of 0.15 ± 0.02 was used to calculate oxygen fugacity based on the method of Kress & Carmichael (1991), returning Δlog fO_2 (QFM) = −0.1, in agreement with oxygen fugacity conditions calculated for the 2021 Fagradalsfjall eruption (QFM − 0.1 (± 0.5), Kahl *et al.*, 2023). Full details of the olivine modelling and initial conditions are reported in the Supplementary Material. The crystallographic orientation of olivine crystals was determined to account for diffusion anisotropy by using electron backscatter diffraction (EBSD) on the JEOL FEG-SEM JSM-IT800 at the Electron microscopy lab for GeoMaterials at Heidelberg University (see Supplementary Material and SDT12).

Plagioclase diffusion modelling

Diffusion of trace elements in plagioclase, such as Mg, is not controlled simply by concentration gradients directly. Rather, the chemical potential gradient is strongly coupled to the anorthite content. This can be approximated using trace-element partition coefficients and their dependence on the anorthite content (Mutch *et al.*, 2022). The dependence of An content in the partition coefficient for Mg into plagioclase may vary between volcanic systems (Moore *et al.*, 2014). Following the approach of Moore *et al.* (2014) and Mutch *et al.* (2021), we calculated the slope (A_{Mg}) and intercept (B_{Mg}) of the Mg partitioning relationship for the 2022–2023 Fagradalsfjall volcanic system. The plagioclase DFENS modelling approach numerically solves the diffusion equation of Costa *et al.* (2003). We use the Mg in plagioclase diffusion coefficient parameterization and covariance matrix of Mutch *et al.* (2021), which uses the diffusion coefficient data of Faak *et al.* (2013). See Mutch *et al.* (2021) for more details.

A total of 43 and 71 profiles were analysed in 40 and 59 plagioclase crystals from the 2022 and 2023 Fagradalsfjall eruption, respectively. In total, 57 plagioclase crystals showed Mg disequilibria at the crystal edges (20 profiles from the 2022 eruption and 37 profiles from the 2023 eruption), which we subsequently modelled by DFENS. Some of the plagioclase profiles from the 2022 (n = 23) and 2023 (n = 34) eruptions were not modelled using DFENS because they did not show prominent Mg diffusive disequilibrium beyond analytical uncertainties or resolution (Bradshaw & Kent, 2017). It is likely that these crystals were exposed to the carrier melt shortly before eruption, suggesting that there was insufficient time to produce an observable Mg disequilibrium at the rim (Fig. S27). Full details on plagioclase modelling parameters can be found in the Supplementary Material.

RESULTS

Petrography

The eruptive products from the 2022 and 2023 Fagradalsfjall eruptions show comparable petrographic features. Tephra and lava samples are slightly phyric to the naked eye, with crystal abundances approximately <3–5 vol% based on visual estimates. In order of abundance, samples contain crystals of plagioclase, olivine, clinopyroxene, and Cr-spinel (Fig. 2A and B). For comparison, the crystal cargo of the 2021 eruptive products is characterized by ∼10 vol% macrocrysts of plagioclase, olivine, clinopyroxene, and Cr-spinel (Halldórsson *et al.*, 2022; Marshall *et al.*, 2024). Following the crystal size classification of Zellmer (2021), plagioclase crystals are found as macrocrysts (>500 μm in length) and mesocrysts (100–500 μm in length), whereas olivine, clinopyroxene, and Cr-spinel crystals mostly occur as mesocrysts in both 2022 and 2023 eruptive products. The only exception to this applies to sample G20220806–3 from the 2022 eruption, in which clinopyroxene macrocrysts were found. In the glass, we observe microcrysts (<100 μm in length) of plagioclase and olivine, present in variable quantities depending on the amount of cooling following eruption. The tephra glass, rapidly quenched in air, is microlite-free while quenched lavas have microlite-rich glass (Fig. 2C–H). Plagioclase macrocrysts are euhedral and characterized by relatively thick rims (10–30 μm), also visible in the rapidly quenched tephra samples (Fig. 2C and D and Fig. S24). Olivine mesocrysts are subhedral to euhedral (Fig. 2E and F). Clinopyroxene mesocrysts, often found in glomerophyric clots together with olivine and plagioclase, are subhedral to euhedral (Fig. 2G and H). All mineral phases contain glassy silicate melt inclusions, up to 100 μm in diameter (Fig. 2C).

The composition of the crystal cargo

Plagioclase macrocrysts have large high-anorthite (An) cores, characterized by complex or patchy An zoning, surrounded by more evolved rims (Fig. 2C and D). Plagioclase macrocryst cores from the 2022 and 2023 products have An contents between

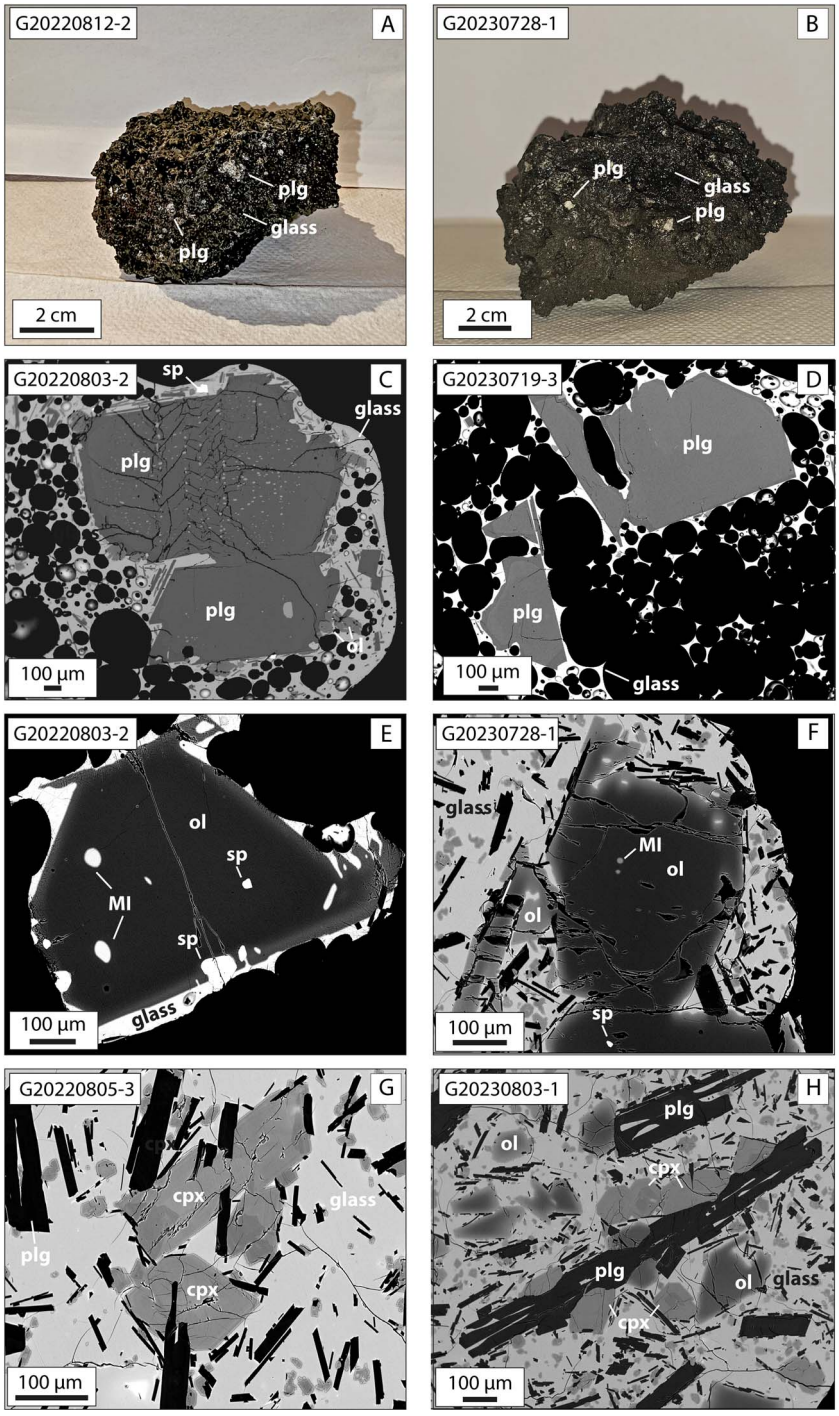

Fig. 2. Petrographic characteristics of the 2022 (left column) and 2023 (right column) Fagradalsfjall products. (**A**, **B**) Photo of a hand-specimen sample of quenched lava from the (**A**) 2022 and (**B**) 2023 eruption. Note the plagioclase (plg) macrocrysts and the glassy crust. (**C**, **D**) BSE image of a plagioclase macrocryst in a tephra sample from the (**C**) 2022 and (**D**) 2023 eruption. Note the glassy melt inclusions (MIs) and the relatively thick plagioclase rims in both images. (**E**, **F**) BSE image of olivine (ol) mesocryst in (**E**) a tephra sample from the 2022 eruption and (**F**) quenched lava from the 2023 eruption. Note spinel (sp) and silicate melt inclusions in both images. (**G**, **H**) BSE image of clinopyroxene (cpx) in quenched lava samples from the (**G**) 2022 and (**H**) 2023 eruption. Note the sector zoning in the pyroxenes and their occurrence as mesocrysts in glomerophyric clots.

$An_{79–90}$ and $An_{84–89}$, respectively, with most compositions (74%) with $An_{84–89}$. Plagioclase macrocryst rims are more evolved in the 2022 ($An_{73–87}$) and 2023 ($An_{74–82}$) products, with most compositions (79%) between $An_{76–82}$ (Fig. 3A). Plagioclase compositions during the 2022 and 2023 Fagradalsfjall eruptions are comparable and do not vary through time in either eruption (Fig. 3A). The major element composition of plagioclase macrocrysts from the 2022 and 2023 Fagradalsfjall eruptions resemble those found in the 2021 products, in which most of the plagioclase cores exhibit $An_{84–90}$ throughout the eruption (Fig. 3A; Marshall *et al.*, 2024). Plagioclase core compositions are also comparable to those erupted during the 2023–2024 eruptions at Sundhnúksgígar in Svartsengi (Matthews *et al.*, 2024) and during 800 to 1240 AD Fires across the RP (Fig. S5A) (Caracciolo *et al.*, 2023).

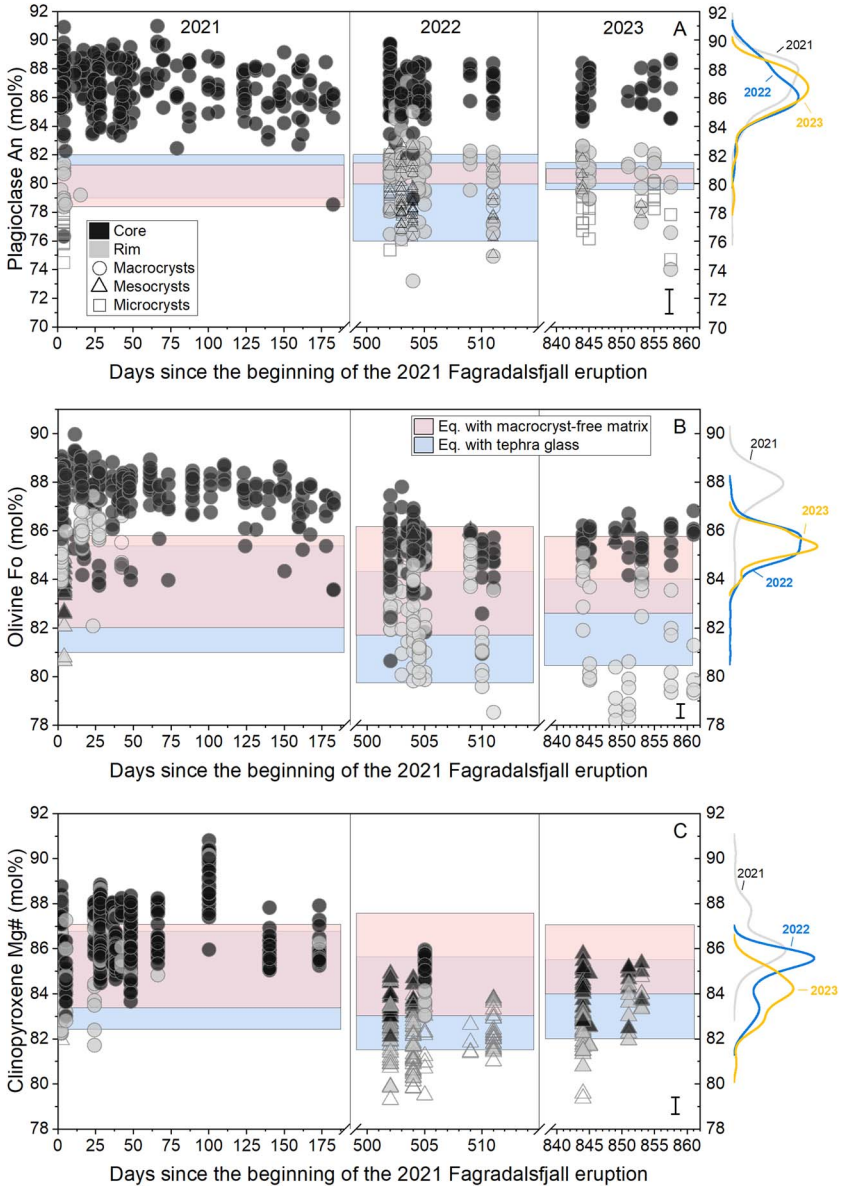

Fig. 3. (**A**–**C**) Time series of the chemical composition of the crystal cargo erupted during the 2021, 2022 and 2023 Fagradalsfjall eruptions as a function of days that passed since the beginning of the 2021 Fagradalsfjall eruption. (**A**) Plagioclase anorthite [An =100xCa_{mol}/(Ca + Na + K)$_{mol}$] (**B**) olivine forsterite [Fo =100 × Mg_{mol}/(Mg + Fe_{Tot})$_{mol}$] and (**C**) clinopyroxene Mg# [Mg# = 100 × Mg_{mol}/(Mg + Fe_{Tot})$_{mol}$]. When possible, measured compositions are divided into crystal groups (macrocryst, mesocryst and microcrysts) and textural groups (core and rim). The error bar in each panel in the bottom right corner indicates the 2σ precision based on repeated analyses of secondary standards (see SDT7–9). Curves on the right side of each figure indicate kernel density estimations (KDEs) of mineral cores, built using Scott's rule (Scott, 2010), coloured according to the eruption. Data from the 2021 Fagradalsfjall eruption are from Halldórsson *et al.* (2022) and Marshall *et al.* (2024). Coloured rectangles indicate mineral compositions in equilibrium with tephra glass (light blue) and macrocryst-free matrix (light pink) compositions for the different eruptions. Plagioclase equilibrium was calculated using the model of Neave & Namur (2022). Olivine and clinopyroxene equilibrium was achieved by using a Fe–Mg Kd in the range 0.27–0.33 (Roeder & Emslie, 1970) and 0.24–0.30 (Putirka, 2008), respectively. In B, we also include olivine core and rim compositions analysed for the diffusion work. Note the two breaks in the horizontal axes and the different major and minor tick scales for the different eruptions.

Olivine macrocrysts exclusively exhibit normal zoning, with low-Fo rims that overgrow high-Fo cores (Fig. 2E and F). Olivine cores from the 2022 and 2023 eruptions range from $Fo_{81–88}$ and $Fo_{84–87}$, respectively, while rims are in the range $Fo_{78–87}$ and $Fo_{77–85}$, with most core (84%) and rim (77%) compositions clustering between $Fo_{84–86}$ and $Fo_{80–85}$ (Fig. 3B). We observe six more primitive olivine cores at the start of the 2022 eruption, with compositions similar to those erupted in 2021. Aside from this, the composition of olivine cores remains consistent throughout the 2022 and 2023 eruptions. These compositions differ from those found in the 2021 eruption. During 2021, most of the olivine cores were in the range $Fo_{87–89}$ (Marshall *et al.*, 2024), more primitive than those erupted in 2022 and 2023 (Fig. 3B). Additionally, unlike the 2021 crystal cargo (Kahl *et al.*, 2023), reverse and complex-zoned olivines are absent in the 2022 and 2023 eruptions. Olivine cores from the 2021–2023 Fagradalsfjall eruptions are more primitive compared to those from the 2023–2024 eruptions at Sundhnúksgígar ($Fo_{75–86}$, Matthews *et al.*, 2024) and the 800 to 1240 AD fires ($Fo_{73–86}$, Caracciolo *et al.*, 2023) (Fig. S5B).

Clinopyroxene mesocrysts show either sector zoning or oscillatory zoning (Fig. 2G and H). Their composition in both the 2022 and 2023 products ranges between Mg#79–86, with

75% of clinopyroxene crystals being in the range Mg#82–85. The composition of clinopyroxene mesocrysts does not change over the course of the 2022 and 2023 eruptions. However, they are more evolved than clinopyroxene from the 2021 eruption (Fig. 3C). In 2021, clinopyroxene occurred as macrocrysts and they were in the range Mg#85–88, with some compositions reaching Mg#90 (Marshall *et al.*, 2024). Clinopyroxene macrocrysts are found in sample G20220806-3 and are in the range Mg#83–86 (Fig. 3C), within the range of macrocrysts from the 2021 eruption. In the eruptive products of the 800 to 1240 AD Fires, clinopyroxene occurred as macrocrysts and mesocrysts and they were overall more evolved than those from the 2021–2023 Fagradalsfjall eruptions (Caracciolo *et al.*, 2023). In the lavas from the 2023–2024 eruptions at Sundhnúksgígar, clinopyroxene occurs as mesocrysts and they are in the range Mg#66–81 (Fig. S5C; Matthews *et al.*, 2024).

Major element composition of the lavas

Lavas erupted in the 2022 and 2023 Fagradalsfjall eruptions have comparable major element compositions (Fig. 4 and Fig. S5). The quenched lava glass has MgO and TiO_2 contents between 6.4–8.2 wt% and 1.2–2.0wt %, respectively, with tephra glasses being slightly more primitive (MgO 7.3–8.2 wt%) than glasses from quenched lavas (MgO 6.4–7.8 wt%). Macrocryst-free matrix compositions are more primitive than the glasses, with MgO contents between 8.3–8.9wt % and 8.6–8.7wt % in samples from the 2022 and 2023 eruptions, respectively (Fig. 4). These ranges are very similar to the whole-rock MgO concentrations, which vary from 8.4 to 8.7 wt%. We do not observe any clear temporal variation in major element composition over the course of the two eruptions (Fig. S6).

The composition of the macrocryst-free matrix for the 2021, 2022, and 2023 eruptions display similar MgO contents, whereas the 2022 and 2023 tephra glasses have lower MgO contents compared to the 2021 tephra glass. Lavas erupted in 2021 are more primitive than any 2022 and 2023 lava and displayed large variations in MgO, SiO_2, and K_2O/TiO_2 over the course of the eruption (Marshall *et al.*, 2024). For comparison, the first four lavas from the 2023 to 2024 eruptions at Sundhnúksgígar and from the 800 to 1240 AD Fires are both more evolved (MgO 6–8.5 wt%) than the 2021 to 2023 Fagradalsfjall lavas (Fig. S7).

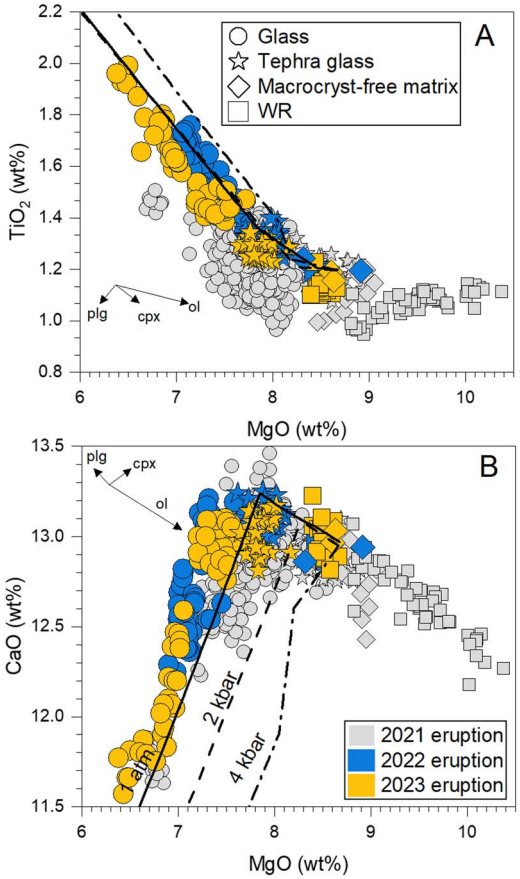

Fig. 4. Major and minor element composition of whole-rock, macrocryst-free matrix and matrix glass from the 2022 and 2023 Fagradalsfjall eruptions. (**A**) MgO versus TiO_2 and (**B**) MgO versus CaO. Comparative data from the 2021 Fagradalsfjall eruption are from Halldórsson *et al.* (2022) and Marshall *et al.* (2024). Black arrows indicate vectors of 2% mineral addition of plagioclase (plg), olivine (ol) and clinopyroxene (cpx). Black solid and dashed lines indicate liquid lines of descent calculated using Petrolog 3 (Danyushevsky & Plechov, 2011) at 0.001 kbar, 2 kbar and 4 kbar, starting from the mean macrocryst-free matrix composition for the 2022 and 2023 eruptions. Precision and accuracy based on repeated analysis of secondary standards is smaller than the symbol size.

Minor and trace element composition of the lavas

The WR and macrocryst-free matrix K_2O/TiO_2 ranges from 0.26–0.28 to 0.24–0.26 in samples from the 2022 and 2023 eruptions, respectively, with the 2022 samples exhibiting slightly higher K_2O/TiO_2 values compared to the 2023 samples. The K_2O/TiO_2 does not change coherently over the course of either eruption (Fig. 5A). In contrast, lavas erupted in 2021 display K_2O/TiO_2 ranging from 0.14 to 0.26, which changed systematically throughout the eruption (Marshall *et al.*, 2024). The 2022 lavas have higher K_2O/TiO_2 than any lava erupted after day 50 of the 2021 Fagradalsfjall eruption, and some lavas exceed the K_2O/TiO_2 of any lava erupted during 2021. The 2023 lavas exhibit lower K_2O/TiO_2, similar to the final lavas erupted in 2021 (Fig. 5A). For comparison, the first four lavas from the 2023–2024 eruptions at Sundhnúksgígar show a similar range of K_2O/TiO_2 to the 2021 Fagradalsfjall lavas, 0.12 to 0.26 (Matthews *et al.*, 2024), while lavas from the 800 to 1240 AD Fires have lower K_2O/TiO_2 than the 2021–2023 Fagradalsfjall lavas, ranging from 0.10 to 0.13 (Fig. S7; Peate *et al.*, 2009).

Trace element (TE) concentrations of matrix glasses show comparable variability in the 2022 and 2023 macrocryst-free matrices. Nearly all incompatible elements have identical variabilities, with a relative variability, as calculated in Fig. S8 (see Supplementary Material), of ~20% (Fig. S8). Ni, Cs, and Pb, however, show 30% to 40% variability between samples. For comparison, the relative variability of TEs in the 2021 lavas ranged between 10% and 160%, correlating with incompatibility, where the most incompatible elements displayed the largest variability (Fig. S8) (Marshall *et al.*, 2024).

Incompatible trace elements (ITE) form negative correlations with the compatible elements Ni and MgO (Fig. 6A and correlation matrices in Figs S9–S12). As an example, the 2022 and 2023 data align along two sub-parallel trends in the Ni versus La space. These trends lie along calculated fractional crystallization trajectories (Fig. 6A). This contrasts with what was observed for the 2021 lavas, which form a positive correlation that is best explained by mixing of melts with distinct mantle-derived variability (Fig. 6A and Figs S9–S12; Marshall *et al.*, 2024).

ITE ratios show variability close to that expected from analytical uncertainty in the 2022 and 2023 lavas, with mean La/Yb of 4.7 ± 0.1 (1σ) and 4.4 ± 0.1 (1σ) in lavas from each eruption, respectively (Fig. 5B). The only exception to this is one sample from 2023 erupted on day 866, which shows higher ITE ratios

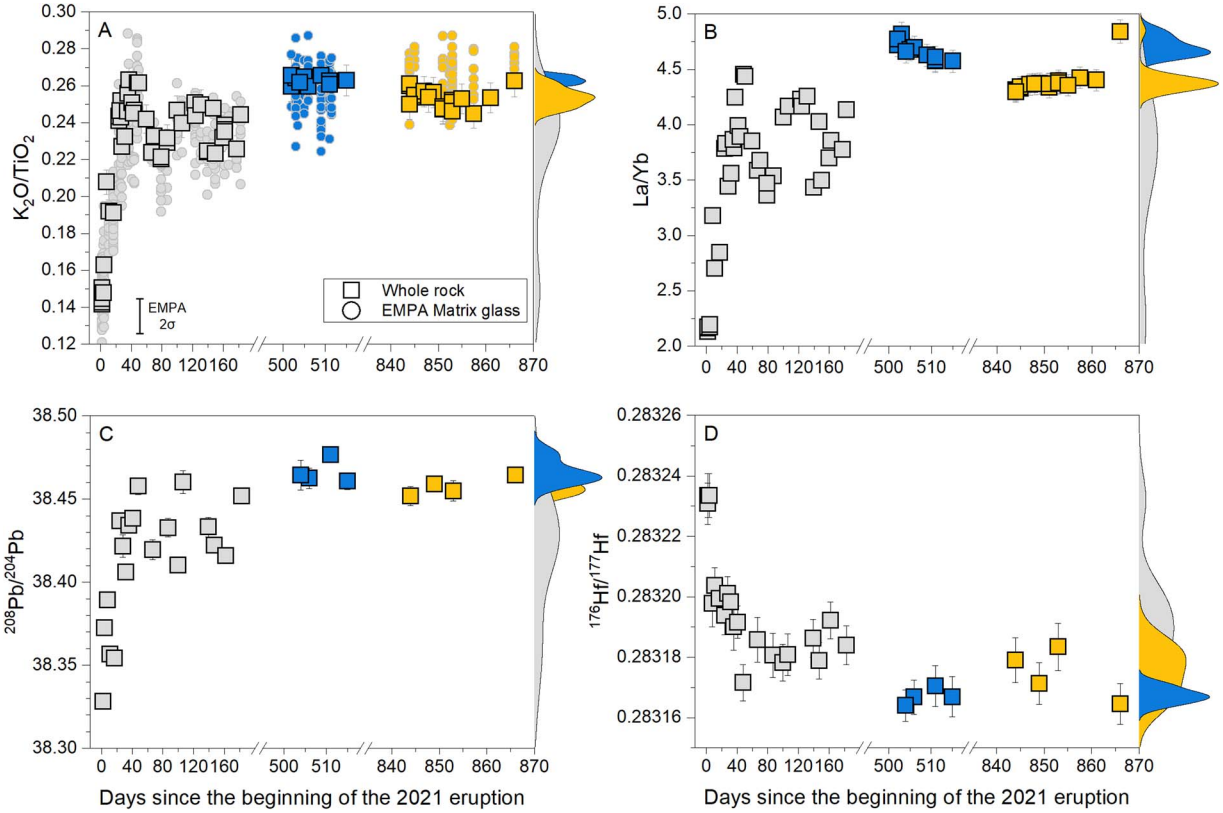

Fig. 5. Time series of different geochemical proxies for the 2021, 2022 and 2023 Fagradalsfjall eruptions. (**A**) time series of $K_2O/TiO2$ for whole rock and matrix glass data (**B**) La/Yb (**C**) $^{208}Pb/^{204}Pb$ (**D**) $^{176}Hf/^{177}Hf$**.** Filled curves on the right side of each figure indicate KDEs of the given geochemical proxy, built using Scott's rule (Scott, 2010), coloured according to the eruption. Data from the 2021 Fagradalsfjall eruption are from Halldórsson *et al.* (2022) and Marshall *et al.* (2024). Note the two breaks in the horizontal axes and the different major and minor tick scales for the different eruptions. Error bars are shown only when they exceed the size of the symbols and represent 2σ precision based on repeated analyses of secondary standards.

compared to the other 2023 samples and more similar to the 2022 samples. This relative homogeneity differs markedly with the lavas erupted in 2021, where La/Yb displayed a wide range from 2.1 to 4.5 (Marshall *et al.*, 2024). We observe weak correlations between time and incompatible trace element ratios (e.g. La/Sm, Zr/Y) for both 2022 and 2023, but because the entire variability of the trends lies very close to analytical uncertainty they cannot be confidently interpreted as temporal trends (Fig. S13). Consequently, ITE ratios display small-to-negligible changes over the course of the 2022 and 2023 Fagradalsfjall eruptions (Fig. S13), especially in comparison with the 2021 lavas.

The lavas from the 2022 and 2023 eruptions show differences in some ITE ratios, with the 2022 lavas, for example, having slightly higher La/Yb, Sm/Yb, and Zr/Y than any 2023 lava (Figs 5B and 6B and Fig. S12). This difference is statistically significant ($p > 0.05$) as confirmed by the Mann–Whitney U test (Fig. S14; Mann & Whitney, 1947). The 2022 lavas have higher ITE ratios than any 2021 lava, whereas the 2023 lavas have similar ITE ratios of the last erupted lavas in 2021 (Figs 5B and 6B). The ITE ratios of the 2022 and 2023 lavas lie along an extrapolation of the binary mixing trend defined by ITE ratios of the 2021 lava (Fig. 6B; Marshall *et al.*, 2024).

Radiogenic isotope composition of the matrix glass

Consistent with the ITE ratios, the $^{87}Sr/^{86}Sr$, $^{143}Nd/^{144}Nd$, $^{176}Hf/^{177}Hf$, and $^{206207208}Pb/^{204}Pb$ ratios of the 2022 and 2023 lavas extend to higher Sr and Pb isotope ratios and lower Nd and Hf isotope ratios than the 2021 lavas (Figs 5 and 6 and Fig. S15).

On average, the 2022 lavas exhibit slightly more radiogenic Sr and Pb isotope ratios and slightly lower Nd and Hf isotope ratios compared to the 2023 lavas (Fig. 6C and D and Fig. S16). The 2023 lavas appear more variable in Sr, Hf, and Pb compared to the 2022 lavas, whereas $^{143}Nd/^{144}Nd$ is relatively invariant across the 2022 and 2023 lavas. Also, one sample erupted at the end of the 2023 eruption (on day 866), has $^{176}Hf/^{177}Hf$, $^{87}Sr/^{86}Sr$, and $^{206207}Pb/^{204}Pb$ similar to the 2022 lavas, consistent with its elevated ITE ratios (Fig. 5C and D and Fig. S16).

Unlike the 2021 lavas, the 2022 and 2023 Fagradalsfjall lavas do not exhibit any significant temporal variability in Sr, Nd, Hf, and Pb isotope compositions beyond analytical uncertainty and do not form consistent or statistically significant trends with one another (Fig. 5C and D and Fig. S16).

Thermobarometry

Clinopyroxene–melt pressures for mesocrysts range between 0–4.5 kbar (0–15 km) and 0–3.0 kbar (0–10 km) in the 2022 and 2023 samples, respectively, with most of the data between 0 and 3 kbar (Fig. 7A). The average crystallization pressure of clinopyroxene mesocrysts is 1.7 ± 1.4 kbar (6 ± 4.7 km) and 1.4 ± 1.4 kbar (4.7 ± 4.7 km) in 2022 and 2023, respectively. We observe a broader pressure distribution in clinopyroxene mesocrysts from the 2022 eruption compared to those from the 2023 eruption (Fig. S17). Crystallization pressures of clinopyroxene macrocrysts found in sample G20220806–3 (day 505) are in the range 1.7 to 4.4 kbar (6–15 km), with a mean of 3.1 ± 1.4 kbar (10.5 ± 4.7 km) (Fig. 7A). We do not observe any temporal variation of clinopyroxene–melt pressures over the course of the 2022 and 2023 eruptions. In

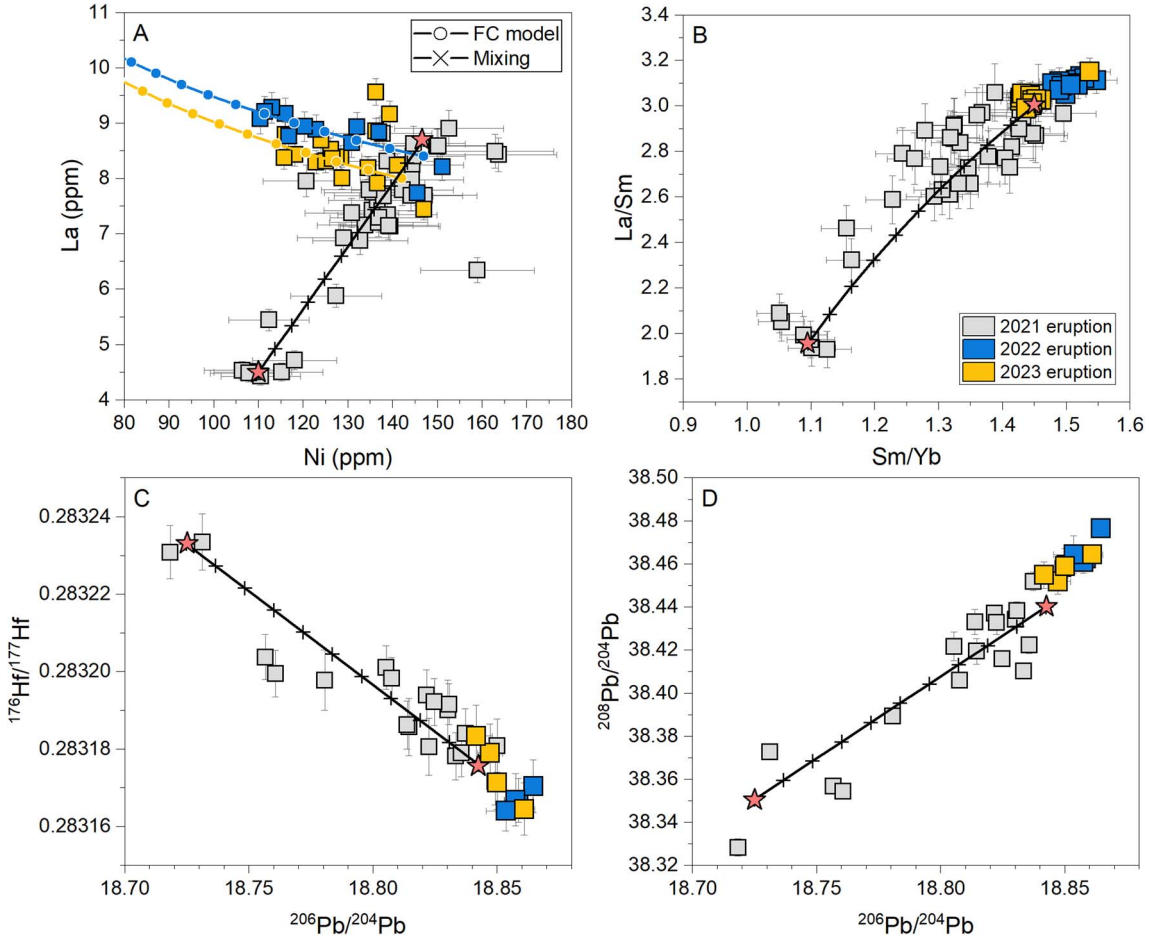

Fig. 6. Bivariant plots of trace element concentrations, trace element ratios and radiogenic isotope ratios for the matrix glass of the 2021, 2022 and 2023 eruptions. (**A**) Nickel concentration versus lanthanum. The 2021 lavas can be reproduced by binary mixing of different end-member compositions (filled red stars, Marshall *et al.*, 2024) indicated by the solid black line. In contrast, a fractional crystallization model (blue and yellow solid lines) reproduces the correlation for the 2022 and 2023 samples. Filled circles along fractional crystallization curves represent 2% crystallization (see Supplementary Section 3 for details on the fractional crystallization model), whereas crosses along mixing curves represent 10% increments. (**B**) Sm/Yb vs La/Sm (**C**) $^{206}Pb/^{204}Pb$ vs $^{176}Hf/^{177}Hf$ (**D**) $^{206}Pb/^{204}Pb$ vs $^{208}Pb/^{204}Pb$. Trace element ratios and radiogenic isotopes of the 2022 and 2023 lavas align along the main mixing trend defined by the 2021 lavas (Marshall *et al.*, 2024), with the 2022 lavas representing the most radiogenic lavas erupted at Fagradalsfjall over the course of the three eruptions. Data from the 2021 Fagradalsfjall eruption are from Halldórsson *et al.* (2022) and Marshall *et al.* (2024). Error bars are shown only when they exceed the size of the symbols and represent 2σ precision based on repeated analyses of secondary standards.

2021, crystallization pressures of clinopyroxene macrocrysts were uniformly between 2.5 and 3.5 kbar (9–13 km), with a mean of 2.9 ± 1.4 kbar (10 ± 4.7 km; Marshall *et al.*, 2024). Overall, clinopyroxene pressures from the 2022 and 2023 eruptions are lower than those from the 2021 eruption, with the exception of pressures of macrocrysts found in sample G20220806–3 that are comparable to those from the 2021 eruption (Fig. 7A). Pressure distributions of clinopyroxene mesocrysts from the 2023 Fagradalsfjall eruption, and to a lesser extent from the 2022 eruption, are comparable to those calculated for the 800–1240 AD Fires in the Reykjanes, Svartsengi, and Krýsuvík volcanic systems, and to those calculated for the first four lavas of the 2023–2024 eruptions at Sundhnúksgígar, with crystallization pressures ranging between 1 and 3 kbar (3.5–10 km) (Fig. S18; Caracciolo *et al.*, 2023; Matthews *et al.*, 2024).

OPAM pressures of quenched lava glasses are in the range 1–2 kbar, with average equilibration pressure of 1.4 ± 1.1 kbar (4.8 ± 3.7 km) and 1.3 ± 1.1 kbar (4.4 ± 3.7 km) in 2022 and 2023, respectively (Fig. 7B). Tephra glasses record slightly higher pressures, with average values of 1.9 ± 1.1 kbar (6.5 ± 3.7 km) and 2.5 ± 1.1 kbar (8.5 ± 3.7 km) in the 2022 and 2023 products, respectively. OPAM pressures of tephra glasses erupted in 2022 and 2023 are lower compared to those calculated in fountaining tephra glasses from the 2021 eruption, which equilibrated at 3.5 to 4.5 kbar (12–15 km) (Fig. 7B). OPAM applied to macrocryst-free matrix compositions from both the 2022 and 2023 eruptions return pressures in the range of 4 to 5.3 kbar (14–18 km), with most of the compositions returning a pressure of 4 ± 1.1 kbar (14 ± 3.7 km). This pressure range agrees with macrocryst-free matrix OPAM pressures for the 2021 eruption (Fig. 7B).

Melt-based thermometry applied to macrocryst-free matrix compositions indicate that the 2022 and 2023 Fagradalsfjall magmas had similar temperatures, within the uncertainties of the thermometers, with a mean OPAM temperature of 1220 ± 10°C (Fig. S19). The mean tephra glass temperature is 1205 ± 10°C, slightly lower than the one calculated for the macrocryst-free matrix compositions but within uncertainty. The 2022 and 2023 macrocryst-free matrices yield a mean temperature similar to that estimated for the 2021 melt (1221 ± 10°C), which is indistinguishable from the temperature of the 2021 tephra glass (1217 ± 10°C) (Fig. S19).

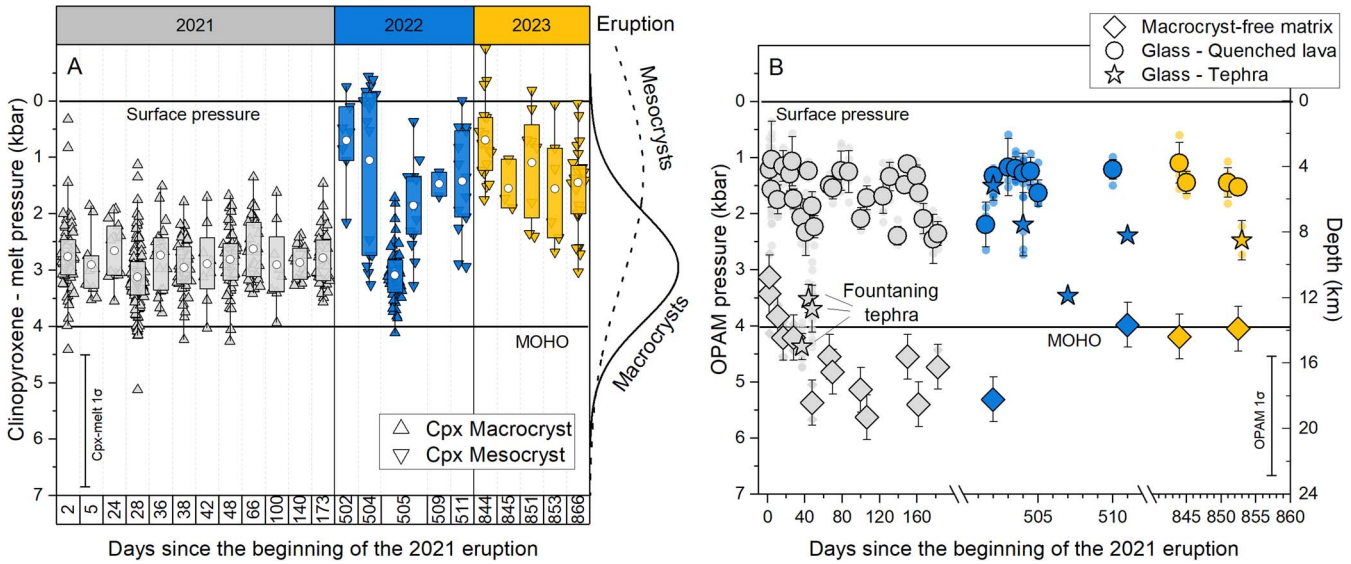

Fig. 7. Barometry results throughout the 2021, 2022 and 2023 Fagradalsfjall eruptions. (**A**) Variation of clinopyroxene–melt pressure estimates since the beginning of the 2021 Fagradalsfjall eruption. Data are plotted as a box plot for each eruption day, in which the boxes represent the interquartile range of the distribution, the white circles represent the mean, and the whiskers represent the 10th and 90th percentiles. Individual clinopyroxene–melt estimates are plotted as filled triangles pointing upwards or downwards, depending on whether the mineral phase is a macrocryst or a mesocryst, respectively. Boxes and data points are coloured according to the eruption. The calibration error of the barometer of ±1.4 kbar (Neave & Putirka, 2017) is indicated in the bottom left part of the figure. Curves at the edge of the figure indicate KDE distributions of cpx–melt pressures for macrocrysts and mesocrysts throughout the three eruptions. KDEs were produced by using a bandwidth of 1.4 to reflect the SEE of the cpx–melt barometer. (**B**) OPAM pressures calculated for matrix glasses (circles), tephra (stars) and macrocryst-free matrix compositions (diamonds). The individual OPAM estimates are indicated with small and faded symbols, whereas the mean values for each day are indicated with larger symbols. The error bars on the macrocryst-free matrix data points represent the 1σ analytical uncertainty, calculated as the standard deviation of pressure estimates obtained from repeated measurements of a single sample from the 2021 eruption (Marshall *et al.*, 2024). In the glass data points, error bars reflect the 1SD of the population. The calibration error of the barometer of ±1.1 kbar (Higgins and Stock, 2024) is indicated in the bottom right part of the figure. Symbols are coloured according to the eruption. Pressure was converted into depth assuming an average crustal density of 3000 kg/m^3 (Darbyshire *et al.*, 2000; Baxter *et al.*, 2023). Note the two breaks in the horizontal axis and the different major and minor tick scales for the different eruptions.

Diffusion timescale results

Fe–Mg diffusion modelling applied to olivine crystals from the 2022 eruption returns timescales in the range of 0.2 to 31 days, while the 2023 eruption yields timescales of 0.2 to 40 days. (Fig. 8 and Fig. S20). The median timescale of the olivine population is 2.6 days for the 2022 eruption, with an average uncertainty of ±0.28 log units (1σ), and 2.5 days for the 2023 eruption, with an average uncertainty of ±0.17 log units (1σ). In both the 2022 and 2023 eruptions, median olivine timescales show a narrow kernel density estimate (KDE) distribution (Fig. S20), with 97% and 95% of the median timescales being shorter than 30 days, respectively. Most of these timescales, 82% for the 2022 eruption and 84% for the 2023 eruption, are shorter than 1 week. In 2021, olivine diffusion timescales ranged between 2 days and 1800 days, with only 30% and 6% of the timescales being shorter than 30 days and 7 days, respectively (Kahl *et al.*, 2023). With a median timescale of 115 days, the olivine timescales from the 2021 Fagradalsfjall eruption are significantly longer compared to 2022 and 2023 olivine timescales (Fig. 8 and Fig. S21; Kahl *et al.*, 2023). However, we note that the 2021 olivine timescales reflect a different magmatic process compared to the 2022 and 2023 olivine timescales (see discussion). We do not observe any correlation between olivine timescales and olivine compositions (Fig. S22).

Diffusion modelling of Mg zoning in plagioclase crystals shows timescales ranging from 6 days to 1294 days (~3.6 years) for the 2022 eruption, and from 1 day to 262 days (~9 months) for the 2023 eruption (Fig. 8). The median timescale of the plagioclase population is 169 days for the 2022 eruption, with an average uncertainty of ±0.33 log units (1σ), and 14 days for the 2023 eruption, with an average uncertainty of ±0.40 log units (1σ). For the 2022 eruption, plagioclase diffusion timescales exhibit a unimodal KDE distribution (Fig. S20), with most of the timescales being between 100 and 400 days. In 2022, 55% of the median timescales are shorter than 6 months and 5% shorter than 1 week. In contrast, the 2023 samples show a bimodal KDE distribution (Fig. S20), with 91% of the median timescales being shorter than 6 months and 44% shorter than 1 week. During the 2021 eruption, 76% of plagioclase timescales are shorter than 6 months with a median timescale of 91 days (Fig. 8 and Fig. S20; Kahl *et al.*, 2023). We do not observe any correlation between plagioclase timescales and plagioclase compositions (Fig. S23).

We find a mismatch in the histogram and KDE distributions of diffusion timescales calculated for olivine and plagioclase crystals in the 2022 and 2023 samples. In the 2022 samples, the plagioclase timescales are shifted towards longer durations (40–1000 days) compared to the olivine timescales (<30 days). In the 2023 samples, plagioclase timescales exhibit a broader range compared to olivine timescales, with similarities observed only in the range of 1–20 days (Fig. 8 and Fig. S20).

DISCUSSION

Geobarometry evidence for stalled or slow magma ascent

The results of the barometric calculations reveal changes in magma storage and crystallization depths within the Fagradalsfjall volcanic system over time. Tephra glass and macrocryst-free matrix compositions are more likely to preserve pre-eruptive magma storage pressures as they are unaffected by near-surface crystallization, unlike quenched lavas (Caracciolo

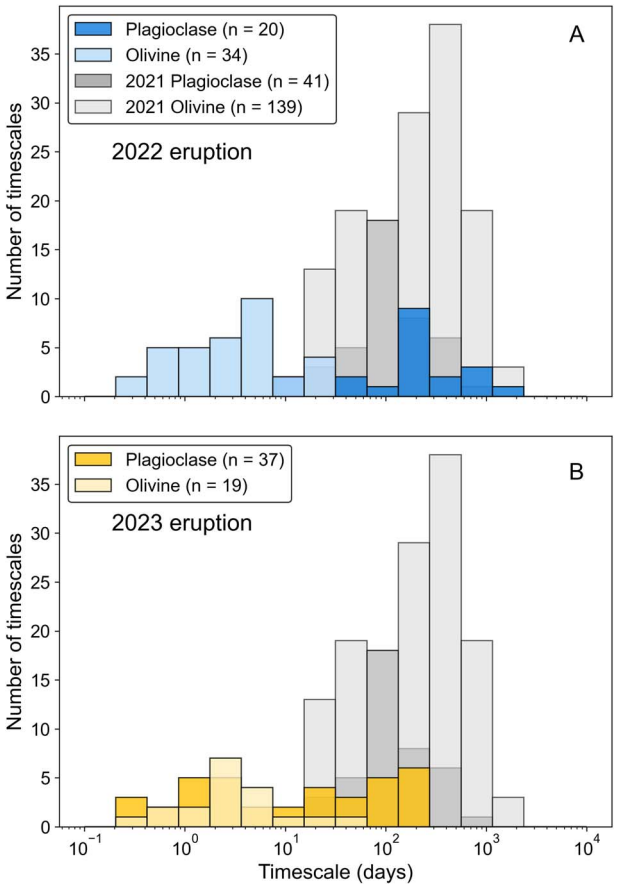

Fig. 8. Histogram distribution of olivine and plagioclase diffusion modelling results for the (**A**) 2022 and (**B**) 2023 Fagradalsfjall eruptions Median timescales are reported in the logarithmic space and histograms are coloured according to the eruption and whether they reflect plagioclase (darker colour) or olivine (lighter colour) distributions. Dark grey and light grey histograms indicate timescale distributions calculated for the 2021 Fagradalsfjall eruption for plagioclase and olivine crystals, respectively (Kahl *et al.*, 2023). KDE plots of median timescale data are shown in Fig. S20.

et al., 2023). Macrocryst-free matrix compositions reflect the melt composition during the early stages of magma evolution, before the crystallization of mesocrysts and microcrysts, unless there is significant rim growth around the macrocrysts. OPAM pressures from macrocryst-free matrix compositions consistently record deep equilibration pressures at 14 ± 3.7 km depth during the 2022–2023 eruptions, consistent with OPAM barometry, melt inclusion saturation pressures and gas measurement results from the 2021 eruption (Halldórsson *et al.*, 2022; Marshall *et al.*, 2024). Considering the crustal structure under the Reykjanes Peninsula (Jenkins *et al.*, 2025), this indicates that the deep magmatic source remained at near-Moho depths throughout the 2021, 2022, and 2023 Fagradalsfjall eruptions (Fig. 7B). The existence of a near-Moho molten region is further supported by seismic imaging of the upper mantle beneath the Reykjanes Peninsula (Jenkins *et al.*, 2025). Jenkins *et al.* (2025) interpret seismic velocities in the sub-Moho region as a thick partially molten mantle transition zone, made of cumulate gabbros and high-melt fraction sills, consistent with petrological observations indicating a near-Moho magma reservoir during the 2021–2023 Fagradalsfjall eruptions (Jenkins *et al.*, 2025).

Clinopyroxene mesocrysts, which are in chemical equilibrium with carrier melts (see following section), formed at a range of crustal depths during 2022 and 2023 (Fig. 7A). This contrasts with persistent lower-crustal crystallization depths of clinopyroxene macrocrysts observed in 2021 (Marshall *et al.*, 2024) and the few clinopyroxene macrocrysts found in one sample from 2022. This is further supported by OPAM pressures calculated for tephra glass compositions, which also indicate variable melt equilibration depths before and/or during the 2022 and 2023 eruptions (Fig. 7B). Overall, we suggest that the 2022 and 2023 magmas originated from a deep magmatic source at near-Moho depths before the crystallization of mesocrysts and microlites, similar to the observations from the 2021 eruption. However, unlike the 2021 magmas, those from 2022 and 2023 underwent cooling after leaving the near-Moho magma domain, marking a distinct contrast to observations from the 2021 Fagradalsfjall eruption. In 2021, magmas ascended directly from near-Moho depths with minimal or no stalling during magma ascent (Halldórsson *et al.*, 2022; Marshall *et al.*, 2024). These results could be explained by two different end-member scenarios: magma crystallization in an incipient mid-crustal reservoir or within the ascending dike during slow ascent, or possibly a combination of both.

In the first scenario, the 2022 and 2023 magmas underwent crystallization in a mid-crustal reservoir, where the mesocryst population formed. This scenario is supported by several observations. First, the clinopyroxene—pressure distribution of mesocrysts from the 2022 and 2023 Fagradalsfjall eruptions encompass a wide range of pressure, similar to findings from the 2023–2024 eruptions at Sundhnúksgígar in Svartsengi (Fig. S18), where a mid-crustal magma domain has been inferred by both geophysical (Sigmundsson *et al.*, 2024; Parks *et al.*, 2025) and petrological studies (Matthews *et al.*, 2024). Second, the tephra glass compositions from the 2022 and 2023 eruptions show lower MgO contents (Fig. 4) and slightly lower melt temperatures (Fig. S19) compared to most tephra glass composition from the 2021 fountaining phase. In contrast, the macrocryst-free matrix compositions and their calculated temperatures remain consistent throughout the 2021–2023 eruptions (Fig. S19). This further supports the idea that the 2022 and 2023 Fagradalsfjall magmas experienced crustal cooling prior to eruption, unlike the magma from 2021. (Pedersen *et al.*, 2022, 2024) Third, the distribution of volcanic tremor measured in the final part of the 2021 Fagradalsfjall eruption is consistent with a dike connected to a sill at ~5 km depth (Soubestre *et al.*, 2025), suggesting that a mid-crustal reservoir may have formed towards the end of the 2021 Fagradalsfjall eruption. However, if this scenario is correct, we recognize that the 2022 and 2023 magmas likely spent little time (hours to days) in the mid-crust before erupting. Unlike its neighbouring volcanic systems, the upper to middle crust under Fagradalsfjall is expected to be relatively cold, indicated by the lack of an active geothermal system and (Jenkins *et al.*, 2025) ~7000 years hiatus in eruptive activity (Einarsson *et al.*, 2023; Jenkins *et al.*, 2025). Under such relatively cold crustal conditions, magmas are expected to cool efficiently during storage. Autocrystic macrocrysts are expected to form during prolonged storage, as for example seen in the eruptions at Sundhnúksgígar (Matthews *et al.*, 2024). If prolonged storage had occurred, the OPAM pressure of the 2022 and 2023 macrocryst-free matrix compositions would have shifted from near-Moho depths to shallower levels. However, this shift is not observed, suggesting limited residence time in this mid-crustal magma reservoir scenario.

The second scenario envisions mesocryst crystallization within the dike during slower magma ascent compared to 2021. This

interpretation is primarily supported by the wide range of clinopyroxene–melt and tephra glass OPAM pressures (Fig. 7), which indicate crystallization at variable depths during magma ascent through the crust. The absence of a strong mid-crustal crystallization signature in both clinopyroxene–melt and tephra glass OPAM pressures, unlike for example in samples from the medieval eruptions (Caracciolo *et al.*, 2023), supports the idea of crystallization across the crust during slower magma ascent. Additionally, the 2022 and 2023 trace element concentrations of macrocryst-free matrix compositions preserve evidence of magma fractionation from a 2021-type lava (see discussion below). Magma stalling in a mid-crustal reservoir would have homogenized this variability, preventing its preservation in the erupted products. Finally, olivine diffusion timescales suggest that the pre-eruptive 2022 and 2023 dikes spent most of their time ascending from near-Moho depths to mid-crustal depths, with only a few days required for the magma to reach the surface from mid-crustal depths after the detection of geophysical precursors (i.e. seismicity and ground deformation) (see discussion below). During this relatively slow ascent through the lower crust, mesocrysts could have formed.

To summarize, we believe that both scenarios, or a combination of them, are plausible, and our dataset does not allow us to distinguish between them definitively. Petrology studies of the 800–1240 AD Fires (Caracciolo *et al.*, 2023) and the 2023–2024 eruptions at Sundhnúksgígar (Matthews *et al.*, 2024) strongly highlight the control of mature mid-crustal magma domains on volcanic eruptions beneath the RP. Although the physical mechanisms underlying the formation of a mid-crustal magma domain remain unclear, our data suggest a temporal evolution in how magmas were processed underneath the Fagradalsfjall plumbing system during the 2021–2023 eruptions. This evolution could reflect either the incipient or early-stage development of a mid-crustal magma reservoir, or a slower magma ascent in the lowermost parts of the crust.

The origin of the crystal cargo

The 2021 Fagradalsfjall crystal cargo is dominated by macrocrysts of plagioclase, olivine and clinopyroxene. The cores of these crystals are found to be antecrystic (Davidson *et al.*, 2007), in major element disequilibrium with the carrier melts, suggesting that they were disaggregated from crystal mush horizons in the lower crust and subsequently incorporated by the ascending dike into the Fagradalsfjall magmas. In contrast, the macrocryst rims are interpreted to be autocrystic—crystallizing directly from the host magma (Marshall *et al.*, 2024).

We evaluated the genetic relationships between the 2022 and 2023 crystal cargo and erupted melts by testing the degree of equilibrium between mineral phases and carrier melts, represented by tephra glass and macrocryst-free matrix compositions (Fig. 3). The 2022 and 2023 olivine ($Fo_{84–86}$) and clinopyroxene (Mg#82–86) mesocrysts display comparable compositions in the two eruptions and are more evolved than macrocrysts found in the 2021 products ($Fo_{86–89}$, Mg#85–90, Marshall *et al.*, 2024). Olivine and clinopyroxene mesocrysts are in major-element equilibrium with tephra glass and macrocryst-free matrix compositions (Fig. 3B and C). Specifically, olivine cores likely crystallized from a melt with a composition similar to the macrocryst-free matrix, a melt composition that equilibrated at near-Moho depths, while olivine rims crystallized from a melt represented by the tephra glass, most likely at mid-crustal depths (cf. 6.1). These mineral–melt relationships suggest that the olivine and clinopyroxene crystals are genetically related to the erupted magmas and are true autocrysts, crystallizing directly from the carrier melts. Conversely, plagioclase macrocryst cores from 2022 and 2023 exhibit compositions similar to those erupted in 2021 ($An_{84–90}$) and are not in major element equilibrium with the carrier melts (Fig. 3A). Plagioclase–melt phase equilibrium is influenced by various factors, such as pressure, temperature, melt composition, and water activity (e.g. Namur *et al.*, 2011), but it is believed that high-An (An>80) plagioclase crystallizes from lower K_2O and higher CaO melts with high liquidus temperature (Grove *et al.*, 1992; Shorttle & Maclennan, 2011), which does not apply to the carrier melts of the 2022 and 2023 eruptions. These observations suggest that plagioclase macrocryst cores did not crystallize from the carrier melts and were likely disaggregated and introduced to the magma from mush layers. In contrast, plagioclase rims are in major element equilibrium with the carrier melts. These findings indicate that after being disaggregated, plagioclase cores were incorporated into the carrier melts from which the plagioclase rims crystallized.

Olivine crystals are interpreted as autocrysts that crystallized from a melt of a similar composition to the macrocryst-free matrix. Further cooling and crystallization during magma ascent and/or short mid-crustal stalling promoted the formation of olivine rims and clinopyroxene mesocrysts. In contrast, plagioclase macrocrysts are identified as antecrysts which likely crystallized in a mush in the deeper parts of the magma plumbing system (Marshall *et al.*, 2024) and were subsequently entrained by the carrier melts, where rim crystallization occurred. The antecrystic nature of plagioclase macrocrysts raises questions about the fate of olivine and clinopyroxene antecrysts, which are largely absent in the 2022 and 2023 crystal cargo as opposed to 2021. To investigate this, we performed Stokes velocity calculations starting from the mean macrocryst-free matrix composition from the 2022 and 2023 eruptions. We based our calculations on a melt density of 2750 kg/m^3 (estimated using DensityX, Iacovino & Till, 2019) and a viscosity of 11 Pa·s, calculated with the model of Giordano *et al.* (2008) at the conditions of the 2022 and 2023 Fagradalsfjall eruptions (T = 1205°C, P = 4 kbar). Our calculations show that olivine and clinopyroxene antecrysts 1 mm in size with a density of 3300 kg/m^3 would settle out of the melt at a rate of approximately 3 m/day. In contrast, plagioclase macrocrysts with a density of 2765 kg/m^3 (Krättli & Schmidt, 2021) are essentially neutrally buoyant in the melt. Different settling velocities could, therefore, explain the coincident presence of plagioclase antecrysts and absence of olivine and clinopyroxene antecrysts. Mid-crustal stalling and/or slower magma ascent from near-Moho depths would have enhanced this mineral segregation process, unlike in 2021, when the connection to the surface was more continuous and less intermittent, especially towards the end of the 2021 eruption.

To summarize, our results show that olivine and clinopyroxene autocrysts, and plagioclase antecrysts represent two different crystal populations. The 2022 and 2023 plagioclase antecrysts are likely much older than the olivine and clinopyroxene autocryst populations. This difference between the 2022 and 2023 olivine and plagioclase crystals is further supported by diffusion timescale data, which show that plagioclase timescales are, on average, significantly longer, on the order of weeks to months, compared to olivine timescales, which are on the order of days. All together, these observations indicate that olivine and plagioclase crystals represent distinct crystal populations in the 2022 and 2023 eruptions, with their diffusion timescales likely reflecting different magmatic processes.

Geochemical evolution of the Fagradalsfjall magma domain following the end of the 2021 Fagradalsfjall eruption

The 2021 eruption at Fagradalsfjall was marked by striking temporal geochemical changes in erupted lava composition, larger than that currently established for the entire 800–1240 AD eruptive period of previous eruptions on the Reykjanes Peninsula (Peate *et al.*, 2009; Halldórsson *et al.*, 2022; Marshall *et al.*, 2024). An outstanding question is how the dynamic plumbing system of the 2021 Fagradalsfjall eruption would continue to change and evolve over time after the end of the eruption, whether stabilizing, undergoing progressive changes, or displaying fluctuating behaviour. Our geochemical results of the 2022 and 2023 eruptions show three major features: (1) limited variability in radiogenic isotope and ITE ratios, (2) radiogenic isotope and ITE ratio compositions similar to the final lavas erupted in 2021, and (3) lava compositions that indicate modest (up to 10%) degrees of crystal fractionation at depth.

The 2021 eruption was interpreted to be sourced from a collection of discrete and compositionally distinct sills (Marshall *et al.*, 2024), but this may not be the case for the 2022 and 2023 eruptions. Given that the compositions of the 2022 and 2023 eruptions are relatively invariant (Fig. 5 and Figs S13-S16), the magma plumbing system supplying these eruptions is likely simpler than that of the compositionally variable 2021 eruption. This is further substantiated by the exponential decline in effusion rate of the 2022 and 2023 eruptions compared to the complex and prolonged effusion in the 2021 eruption (Pedersen *et al.*, 2022, 2024). In volcanic eruptions, exponential declines in effusion rate are usually interpreted to reflect the elastic relaxation of a single inflated magma chamber (Wadge, 1981; Aravena *et al.*, 2020). Therefore, the simple exponential decline in the effusion rates of the 2022 and 2023 eruptions, in contrast to the 2021 eruption, adds to the evidence a single magma chamber as a source. Additionally, because single basaltic magma reservoirs homogenize on a days-to-weeks timescale (Maclennan, 2019), the lack of compositional variability in mantle tracers is also more suggestive of an eruption from a single magma chamber, as also proposed for the evolved (in-caldera) Krafla magmas during the 1975–1984 eruptions (Rooyakkers *et al.*, 2024).

One possibility is that following the end of the 2021 eruption, significant recharge from the mantle source or rearrangement of the near-Moho magma domain structure led to slightly different magma compositions erupted in 2022 and 2023. While the mean composition of the 2022 and 2023 lavas is compositionally distinct from those erupted in 2021 in terms of ITE ratios and radiogenic isotope ratios, their compositions fall along mixing trends that were defined by the 2021 eruption products. For example, in Fig. 6B, the Sm/Yb and La/Sm of the 2022 and 2023 lavas form a trend that is an extension of the binary mixing trend defined by the 2021 lavas. Furthermore, the radiogenic isotope compositions of the 2022 and 2023 lavas lie along extrapolations of the trends established by lavas erupted late in the 2021 eruption (Fig. 6C and D). The shift of the ITE ratios and radiogenic isotope ratios to more enriched compositions (i.e. compositions that reflect the enrichment of incompatible elements) than the 2021 lavas suggests that the depleted melts that dominated the first weeks of the 2021 eruption are not as prominent in the 2022 and 2023 eruptions. However, differences in the ITE ratios and radiogenic isotope ratios of the 2022 and 2023 eruptions (2022 lavas being generally more enriched than 2023 lavas) show that the source of these eruptions was not a single homogeneous endmember component, and that depleted melts in the Fagradalsfjall magma domain might not be entirely exhausted. Together, the compositional differences and similarities of the 2022 and 2023 eruptions to the 2021 eruption show that the Fagradalsfjall near-Moho magma domain has stabilized over three years and shows no evidence of new and unobserved melt compositions.

However, a key difference between the 2022–2023 eruptions and the 2021 eruptions is evidence for modest crystal fractionation of the 2022–2023 magmas. Figure 6A shows that the compositional variation of the 2022–2023 macrocryst-free matrix lies along a fractional crystallization trend. Unlike the composition of volcanic glass, the composition of macrocryst-free matrix is not affected by the crystallization of microlites or mesocrysts that form during magma ascent or on the surface. Changing the composition of the macrocryst-free matrix requires crystal–melt separation, such as crystal settling, which is a slow process relative to the timescale of an eruption and lava flows. For example, a 100 μm diameter olivine microlite sinks only 2.4 cm/day (same physical parameters and magma compositions as in Section 6.2). Therefore, crystal fractionation likely took place at depth over a longer interval of time than the eruption timescale. The magnitude of fractional crystallization that occurred is modest, but detectable. Starting from a 2021 lava-type composition, we calculated that no more than ∼10% fractionation took place (Fig. 6A and Section 3 in the Supplementary Material for modelling calculations). Given that ITE ratios and radiogenic isotope ratios are relatively uniform throughout both the 2022 and 2023 eruptions, it is possible that magmas were stored within a single magma chamber that underwent convective homogenization and crystal fractionation prior to and during each of the 2022 and 2023 eruptions.

The plagioclase and olivine timescale record: Two distinct magmatic processes preserved in the crystal cargo

The olivine and plagioclase timescales from the 2022 and 2023 samples record two distinct magmatic processes as olivine mesocrysts and plagioclase macrocrysts represent separate crystal populations. These different magmatic processes are also characterized by different timescales, as olivine crystals record short timescales, on the order of days, whereas plagioclase exhibits long and more variable timescales, on the order of weeks to months, up to years. This distinction can be observed in Fig. 9A, where the 2022 and 2023 olivine and plagioclase timescales distribute along two different cumulative curves, beyond timescale uncertainties.

We know that plagioclase macrocrysts represent mush crystals, most of which were incorporated into the 2022 and 2023 magmas upon being eroded from mush layers. We interpret the timescales associated with plagioclase macrocrysts as representing the time interval from mush disaggregation to eruption. Mg disequilibrium in plagioclase modelled in this study was likely established during the disaggregation of plagioclase macrocrysts in different part of the plumbing system and during magma ascent towards the surface. This process occurred in the years, months and days prior to the 2022 and 2023 Fagradalsfjall eruptions. Specifically, four plagioclase macrocrysts from the 2022 eruption capture processes antecedent to the 2021 dike (Dike 1) and possibly before the initial detection of magmatic unrest in the RP (Fig. 9A and B). Based on Kahl *et al.* (2023), one of these plagioclase crystals falls within the priming phase of deep magma accumulation and mush disaggregation whereas three crystals record the transition phase that led to the 2021 eruption (Fig. 9A). These four 2022 plagioclase crystals align closely with the 2021 plagioclase cumulative timescale curve, suggesting that they were

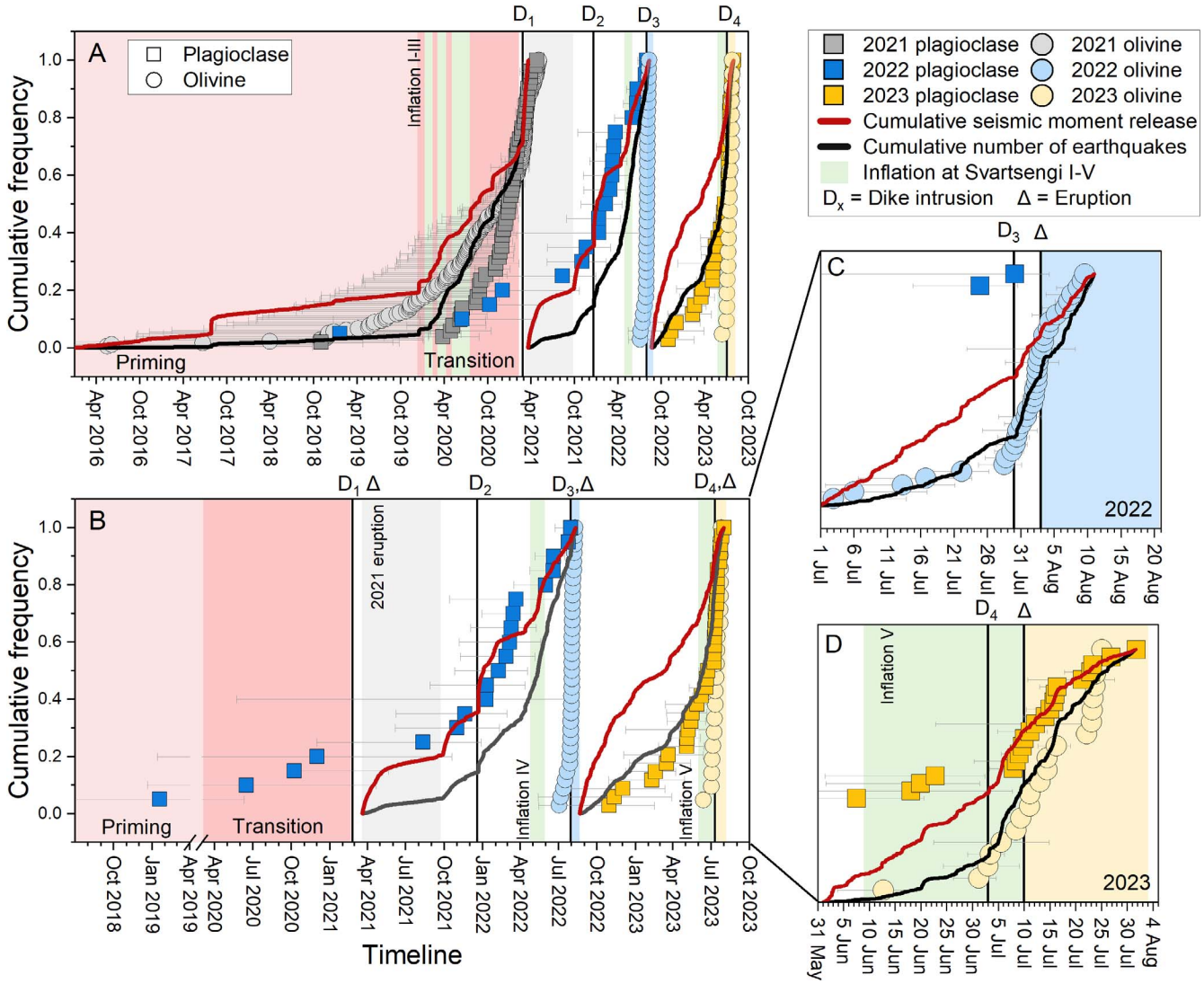

Fig. 9. Diffusion timescales linked to geophysical and geodetic precursors. (**A**) Cumulative distribution of plagioclase and olivine timescales for the 2021, 2022 and 2023 Fagradalsfjall eruptions, allowing comparison between the different eruptions (**B**) Timescale data for the 2022 and 2023 eruptions. The priming and the transition phase leading to the 2021 eruption are indicated with shaded red areas, as defined in Kahl *et al.* (2023). Panels (**C**) and (**D**) offer enlarged views of the time periods in the ~month before the 2022 and 2023 eruptions, respectively. D_x refers to the time of propagation of the different dikes as detected by seismicity. Inflation episodes I to V recorded at Svartsengi are indicated with pale green fields. The onset of each eruption is marked with a delta (Δ) symbol and their duration with coloured shaded areas. The red thick solid line indicates the cumulative seismic moment release, calculated using the expression by Hanks & Kanamori (1979). The black thick solid line indicates the cumulative number of earthquakes. Seismic data were extracted from https://skjalftalisa.vedur.is. Symbols and colours of data points are according to the eruption and the mineral phase. Timescale data from the 2021 Fagradalsfjall eruption are from Kahl *et al.* (2023).

disaggregated and mobilized during the priming and transition phase leading up to the 2021 eruption, but did not erupt until 2022. As discussed in Section 6.2, plagioclase macrocrysts are neutrally buoyant in the Fagradalsfjall magmas as opposed to olivine and clinopyroxene macrocrysts. The preferential buoyancy of plagioclase indicates that some plagioclase disaggregated in 2021 may have remained suspended in the plumbing system after the end of the 2021 eruption, representing recycled crystals that were subsequently picked up during the 2022 eruption. Interestingly, these plagioclase crystals recording timescales antecedent to the 2021 dike are absent in the 2023 products, with plagioclase timescales from the 2023 eruption exclusively pointing to magmatic processes occurring after the end of the 2022 eruption (Fig. 9A and B). This evidence suggests a temporal evolution in crystal-mush disaggregation to eruption timescales during the 2021–2023 Fagradalsfjall eruptions, transitioning from timescales of years prior to the 2021 eruption to timescales of months during the 2022–2023 eruptions. Plagioclase crystals recording the priming and transition phase of the 2021 eruption are becoming scarce and disappearing over time, possibly because they were fully entrained and erupted by the end of the 2022 eruption. This suggests that during the 2022 and 2023 eruptions less energy and time were needed to erode the crystal mush compared to 2021, possibly because it was more loosened, likely due to the 2021 event having triggered and disrupted the bulk of the mush. This interpretation is also supported by observations from Bárðarbunga volcano, where Caracciolo *et al.* (2021) documented a shortening of crystal-mush disaggregation timescales over the Holocene, attributing this variation to the development of a more loosely connected mush system.

Unlike most plagioclase crystals, olivine mesocrysts did not originate from a mush. Instead, they likely crystallized

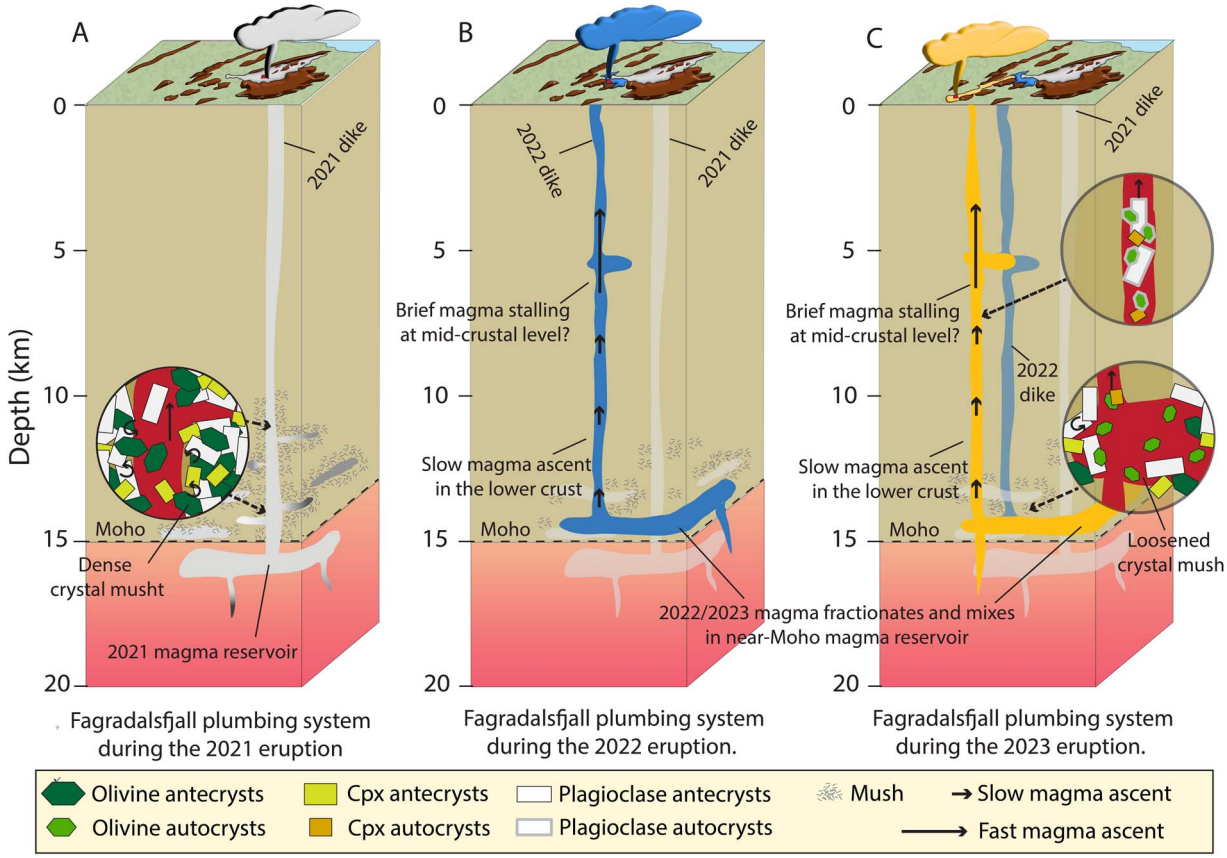

Fig. 10. Cartoon summarizing the magma plumbing system beneath Fagradalsfjall and its temporal evolution from 2021 to 2023 (not to scale). (**A**) Configuration of the plumbing system following the 2021 Fagradalsfjall eruption, with a dike propagating towards the surface from a near-Moho magma domain. Multiple sills of different magma compositions contributed to the 2021 eruption (different shades of grey). Syn-eruptive erosion of crystal mushes in the lower crust and deep magma assembly started in the years before the 2021 eruption. This model summarizes observations from Halldórsson *et al.* (2022), Kahl *et al.* (2023) and Marshall *et al.* (2024). (**B-C**) Following the 2021 Fagradalsfjall eruption, magma started to accumulate and fractionate in a near-Moho magma reservoir, possibly slightly shallower than the 2021 reservoir. A more loosely connected mush network in 2022–2023 compared to 2021 facilitated faster erosion of the mush and faster magma assembly over timescales of months. Combined diffusion modelling, barometry, and geophysical data suggest that the 2022–2023 dikes began propagating from near-Moho depths ~1 month prior to the eruptions, with magma ascending slowly (weeks) through the lower crust. The magmas then breached the uppermost part of the crust within a few days.

from a melt with a composition similar to the macrocryst-free matrix at near-Moho depths. Following this, the olivine Fe–Mg disequilibrium was likely produced by rim growth during magma ascent towards the surface. Therefore, we interpret the olivine timescales as reflecting the timescales of dike opening and propagation from near-Moho depths to the surface. Some plagioclase timescales coincide with olivine timescales, likely representing crystals which were eroded in different parts of the plumbing system**.** This interpretation is further supported by the agreement between pre-seismicity in the weeks preceding the 2022–2023 eruptions (https://skjalftalisa.vedur.is/) and our timescale record, suggesting that olivine timescales are capturing both the duration and the timing of dike opening and propagation from near-Moho depths (Fig. 9C and D). Specifically, the longest olivine timescales preserved in both the 2022 and 2023 datasets are consistently ~1 month, indicating that the dikes must have begun travelling through the crust from near-Moho levels at least ~1 month prior to the 2022 and 2023 eruptions. Following this, the 2022 and 2023 dikes were detected by geophysical precursors (i.e. seismicity and ground deformation) only 4 and 7 days before the 2022 and 2023 eruptions, respectively. According to Parks *et al.* (2023), dike intrusion preceding the 2022 eruption was detected on 30 July 2022, with seismicity suggesting a dike at mid-crustal depths of ~8 km, before quickly ascending to the upper crust at ~3 km depth. The 2022 dike erupted 4 days after the detection of geophysical precursors. In 2023, dike intrusion was detected by seismicity on 3 July 2023 and most of the pre-seismicity was located at depths between 2 and 8 km (https://skjalftalisa.vedur.is/), at a similar depth range as in 2022. The 2023 dike erupted 7 days after the detection of geophysical precursors. Assuming that the dike began traversing the crust from near-Moho depths, our combined timescale, barometry, and geophysical data suggest that the 2022 and 2023 dikes spent most of their time traversing the lower crust (between 8 and 14 km) before being detected at mid-crustal depths by geophysical precursors (Fig. 10). After reaching mid-crustal depths, the 2022 and 2023 dikes rapidly broke through the uppermost crust in a few days, as suggested by both olivine diffusion timescales and geophysical observations (Fig. 9C and D). This marks a sharp difference compared to 2021, when the dike took ~3 weeks to traverse the uppermost part of the crust (Sigmundsson *et al.*, 2022). Overall, this suggests the establishment of a well-defined upper crustal magma pathway prior to the 2022 and 2023 eruptions compared to 2021. This pathway reflects more efficient magma transport from mid-crustal levels to the surface, with advance warning times reduced by 65% to 80% in 2022 and 2023 compared to 2021.

General implications for plume and rift basaltic plumbing systems

Observations from our study hold implications for active basaltic volcanoes worldwide. The temporal evolution of plumbing systems is a crucial factor in understanding how successive eruptions affect the underlying plumbing system over time. First, the temporal decrease of crystal-mush disaggregation timescales from 2021 to 2023 indicates a progressive shortening of unrest timescales. This suggests that the Fagradalsfjall plumbing system is responding more rapidly over time to melt injections from near-Moho depths, processes that are often undetected by geophysical methods (Fig. 9A and B). Such a trend has significant implications for volcanic systems worldwide, as repeated eruptions in close temporal succession could lead to much shorter periods of unrest prior to eruption. Furthermore, our findings highlight the challenges of detecting deep magmatic processes with existing monitoring tools. We showed that the 2022 and 2023 dikes spent most of their time traversing the lower crust, without being detected by geophysical methods. Both observations underscore the importance of deep magmatic processes and the need for enhancing monitoring approaches to detect the deep early phases of magma accumulation and dike propagation at active volcanoes (e.g. Kahl *et al.*, 2023). Whereas seismicity is often used as a primary indicator of magma movement, its effectiveness is reduced in deeper and more ductile parts of the crust, where strain can be accommodated aseismically (Meissner & Strehlau, 1982). This highlights the need to integrate multiple geophysical techniques, including geodetic measurements and electromagnetic methods, to improve detection of deep magma transport. Secondly, there are implications for studying past eruptions, as our data show that timescales derived from the crystal cargo erupted during the later stages of prolonged activity may be biased and do not reflect the entire history of the eruptive period, potentially not including the early priming and transition phases of deep magma assembly. As a result, key information about the deeper and earlier stages of magma assembly, which set the stage for subsequent eruptions, may be underrepresented or completely absent in the crystal record. Such bias is particularly relevant when interpreting diffusion chronometry data, as crystals erupted during the final stage of an eruption may sample only the latest stages of magma storage and ascent. Overcoming such bias can be addressed with a more concerted effort when possible, within the scientific community to identify and analyse deposits that capture the initiation of eruptions or, ideally, the full eruptive sequence. Such an approach would enhance our understanding of past eruptions and provide a more complete picture, uncovering critical information that might otherwise remain hidden.

CONCLUSIONS

Our main findings are:

1) Olivine and clinopyroxene crystals in 2022 and 2023 are primarily autocrysts, indicating that they crystallized from the Fagradalsfjall carrier magmas. In contrast, plagioclase crystals are antecrysts eroded from crystal mushes and did not crystallize from the Fagradalsfjall magmas. This suggests two different crystal populations in the 2022–2023 Fagradalsfjall crystal cargo.
2) The 2021–2023 Fagradalsfjall eruptions were sourced from a persistent deep magma domain located at 14 ± 3.7 km depth. However, during the 2022 and 2023 eruptions, magmas likely stalled at mid-crustal levels within an incipient reservoir or ascended more slowly, a process that was not observed in the 2021 eruptive products.
3) Unlike the 2021 eruption, the 2022 and 2023 Fagradalsfjall lavas display limited geochemical variability and are likely sourced from a single, reasonably well mixed magma reservoir.
4) The incompatible trace element ratios and radiogenic isotope compositions of the 2022–2023 lavas lie along mixing trends established by the compositional variability seen in the 2021 eruption, suggesting little changes in melt compositions within the Fagradalsfjall deep magma domain in three years of eruptions.
5) Plagioclase diffusion timescales, ranging from years to months and days, correspond to mush disaggregation to eruption timescales. These timescales shorten over the course of the 2021–2023 eruptions, suggesting a progressively loosened mush and a faster response of the magmatic plumbing system to deep melt injections, with shorter warning times.
6) Olivine timescales, spanning days to a few weeks, capture the timing and duration of dike opening and propagation during the 2022 and 2023 events from near-Moho depths to the surface. The dikes spent significantly more time traversing the lower crust, while the upper crust was breached in just a few days.
7) The timescales of magma ascent from mid-crustal levels to the surface shortened from 2021 to 2023, indicating the development of more efficient upper-crustal magma pathways.

SUPPLEMENTARY DATA

Supplementary data are available at *Journal of Petrology* online.

ACKNOWLEDGEMENTS

This work was funded by the Icelandic Research Fund grant of excellence #228933-053. A.C. acknowledges Matteo Arre for his help with installing DFENS and the required Python packages. E.J.F.M. acknowledges funding from the MOE Tier 3 Grant InVEST (MOE-MOET32021-0002). Helena Albert, Jordan Lubbers, and an anonymous reviewer are thanked for their constructive comments, which significantly improved the original version of the manuscript. We also thank Adam Kent and Georg Zellmer for their comments and editorial support.

DATA AVAILABILITY

The data supporting this article are available in the Supplementary Materials, organized into 13 supplementary data tables (SDTs). Geochemical data from this article are available in the FAIR EarthChem data repository at this link https://doi.org/10.60520/IEDA/113723.

REFERENCES

Aravena, A., Cioni, R., Coppola, D., de Michieli Vitturi, M., Neri, A., Pistolesi, M. & Ripepe, M. (2020). Effusion rate evolution during small-volume basaltic eruptions: insights from numerical modeling. *Journal of Geophysical Research: Solid Earth* **125**. https://doi.org/10.1029/2019JB019301.

Barsotti, S., Parks, M. M., Pfeffer, M. A., Óladóttir, B. A., Barnie, T., Titos, M. M., Jónsdóttir, K., Pedersen, G. B. M., Hjartardóttir, Á. R.,

Stefansdóttir, G., Johannsson, T., Arason, Þ., Gudmundsson, M. T., Oddsson, B., Þrastarson, R. H., Ófeigsson, B. G., Vogfjörd, K., Geirsson, H., Hjörvar, T., von Löwis, S., Petersen, G. N. & Sigurðsson, E. M. (2023). The eruption in Fagradalsfjall (2021, Iceland): how the operational monitoring and the volcanic hazard assessment contributed to its safe access. *Natural Hazards* **116**, 3063–3092. https://doi.org/10.1007/s11069-022-05798-7.

Baxter, R. J. M. & Maclennan, J. (2024). Influence of magma flux on magma storage depths along the Reykjanes Ridge. *Earth and Planetary Science Letters* **631**, 118633. https://doi.org/10.1016/j.epsl.2024.118633.

Baxter, R. J. M., Maclennan, J., Neave, D. A. & Thordarson, T. (2023). Depth of magma storage under Iceland controlled by magma fluxes. *Geochemistry Geophysics Geosystems* **24**. https://doi.org/10.1029/2022GC010811.

Belart, J. M. C., Pinel, V., Reynolds, H. I., Berthier, E. & Gunnarson, S. R. (2023). Digital elevation models (DEMs) and lava outlines from the 2023 Litla-Hrútur eruption, Iceland, from Pléiades satellite stereoimagesZenodo. https://doi.org/10.5281/zenodo.10133203.

Bindeman, I. N., Deegan, F. H., Troll, V. R., Thordarson, T., Höskuldsson, A., Moreland, W., Zorn, E., Shevchenko, A. V. & Walterr, T. R. (2022). Diverse mantle components with invariant oxygen isotopes in the 2021 Fagradalsfjall eruption, Iceland. *Nature Communications* **13**, 1–12. https://doi.org/10.1038/s41467-022-31348-7.

Bradshaw, R. W. & Kent, A. J. R. (2017). The analytical limits of modeling short diffusion timescales. *Chemical Geology* **466**, 667–677. https://doi.org/10.1016/j.chemgeo.2017.07.018.

Caracciolo, A., Bali, E., Guðfinnsson, G. H., Kahl, M., Halldórsson, S. A., Hartley, M. E. & Gunnarsson, H. (2020). Temporal evolution of magma and crystal mush storage conditions in the Bárðarbunga–Veiðivötn volcanic system, Iceland. *Lithos* **352-353**, 105234. https://doi.org/10.1016/j.lithos.2019.105234.

Caracciolo, A., Kahl, M., Bali, E., Guðfinnsson, G. H., Halldórsson, S. A. & Hartley, M. E. (2021). Timescales of crystal mush mobilization in the Bárðarbunga–Veiðivötn volcanic system based on olivine diffusion chronometry. *American Mineralogist* **106**, 1083–1096. https://doi.org/10.2138/am-2021-7670.

Caracciolo, A., Bali, E., Halldórsson, S. A., Guðfinnsson, G. H., Kahl, M., Þórðardóttir, I., Pálmadóttir, G. L. & Silvestri, V. (2023). Magma plumbing systems and timescale of magmatic processes during historical magmatism on Reykjanes Peninsula. *Earth and Planetary Science Letters* **621**, 118378. https://doi.org/10.1016/j.epsl.2023.118378.

Caracciolo, A., Bali, E., Ranta, E., Halldórsson, S. A., Guðfinnsson, G. H. & Óskarsson, B. V. (2024). Medieval and recent SO2 budgets in the Reykjanes Peninsula: implication for future hazard. *Geochemical Perspectives Letters* **30**, 20–27. https://doi.org/10.7185/geochemlet.2417.

Cashman, K. V., Sparks, R. S. J. & Blundy, J. D. (2017). Vertically extensive and unstable magmatic systems: a unified view of igneous processes. *Science* **355**, 1–9. https://doi.org/10.1126/science.aag3055.

Chakraborty, S. (1997). Rates and mechanisms of Fe–Mg interdiffusion in olivine at 980°–1300°C. *Journal of Geophysical Research* **102**, 12317–12331. https://doi.org/10.1029/97JB00208.

Costa, F., Chakraborty, S. & Dohmen, R. (2003). Diffusion coupling between major and trace elements and a model for the calculation of magma chamber residence times using plagioclase. *Geochimica et Cosmochimica Acta* **67**, 2189–2200. https://doi.org/10.1016/S0016-7037(02)01345-5.

Crank, J. (1979) *The mathematics of diffusion*. Oxford: Oxford university press.

Cubuk-Sabuncu, Y., Jónsdóttir, K., Caudron, C., Lecocq, T., Parks, M. M., Geirsson, H. & Mordret, A. (2021). Temporal seismic velocity changes during the 2020 rapid inflation at Mt. Þorbjörn-Svartsengi, Iceland, using seismic ambient noise. *Geophysical Research Letters* **48**. https://doi.org/10.1029/2020GL092265.

Danyushevsky, L. V. & Plechov, P. (2011). Petrolog3: integrated software for modeling crystallization processes. *Geochemistry, Geophysics, Geosystems* **12**, 1–32. https://doi.org/10.1029/2011GC003516.

Darbyshire, F. A., White, R. S. & Priestley, K. F. (2000). Structure of the crust and uppermost mantle of Iceland from a combined seismic and gravity study. *Earth and Planetary Science Letters* **181**, 409–428. https://doi.org/10.1016/S0012-821X(00)00206-5.

Davidson, J. P., Morgan, D. J., Charlier, B. L. A., Harlou, R. & Hora, J. M. (2007). Microsampling and isotopic analysis of igneous rocks: implications for the study of magmatic systems. *Annual Review of Earth and Planetary Sciences* **35**, 273–311. https://doi.org/10.1146/annurev.earth.35.031306.140211.

Davydova, V. O., Shcherbakov, V. D., Plechov, P. Y. & Koulakov, I. Y. (2022). Petrological evidence of rapid evolution of the magma plumbing system of Bezymianny volcano in Kamchatka before the December 20th, 2017 eruption. *Journal of Volcanology and Geothermal Research* **421**, 107422. https://doi.org/10.1016/j.jvolgeores.2021.107422.

Day, J. M. D., Kelly, S., Troll, V. R., Moreland, W. M., Cook, G. W. & Thordarson, T. (2024). Deep crustal assimilation during the 2021 Fagradalsfjall Fires, Iceland. *Nature* **632**, 564–569. https://doi.org/10.1038/s41586-024-07750-0.

Dohmen, R. & Chakraborty, S. (2007). Fe–Mg diffusion in olivine II: point defect chemistry, change of diffusion mechanisms and a model for calculation of diffusion coefficients in natural olivine. *Physics and Chemistry of Minerals* **34**, 409–430. https://doi.org/10.1007/s00269-007-0158-6.

Dohmen, R., Becker, H. W. & Chakraborty, S. (2007). Fe–Mg diffusion in olivine I: experimental determination between 700 and 1,200°C as a function of composition, crystal orientation and oxygen fugacity. *Physics and Chemistry of Minerals* **34**, 389–407. https://doi.org/10.1007/s00269-007-0157-7.

Einarsson, P. (2008). Plate boundaries, rifts and transforms in Iceland. *Jokull* **58**, 35–58.

Einarsson, P., Eyjólfsson, V. & Rut, Á. (2023). Tectonic framework and fault structures in the Fagradalsfjall segment of the Reykjanes Peninsula Oblique Rift, Iceland. *Bulletin of Volcanology* **85**, 1–17. https://doi.org/10.1007/s00445-022-01624-x.

Faak, K., Chakraborty, S. & Coogan, L. A. (2013). Mg in plagioclase: experimental calibration of a new geothermometer and diffusion coefficients. *Geochimica et Cosmochimica Acta* **123**, 195–217. https://doi.org/10.1016/j.gca.2013.05.009.

Flóvenz, Ó. G., Wang, R., Hersir, G. P., Dahm, T., Hainzl, S., Vassileva, M., Drouin, V., Heimann, S., Isken, M. P., Gudnason, E. Á., Ágústsson, K., Ágústsdóttir, T., Horálek, J., Motagh, M., Walter, T. R., Rivalta, E., Jousset, P., Krawczyk, C. M. & Milkereit, C. (2022). Cyclical geothermal unrest as a precursor to Iceland's 2021 Fagradalsfjall eruption. **15**, 397–404. https://doi.org/NatureGeoscience, 10.1038/s41561-022-00930-5.

Giordano, D., Russell, J. K. & Dingwell, D. B. (2008). Viscosity of magmatic liquids: a model. *Earth and Planetary Science Letters* **271**, 123–134. https://doi.org/10.1016/j.epsl.2008.03.038.

Greenfield, T., Winder, T., Rawlinson, N., Maclennan, J., White, R. S., Ágústsdóttir, T., Bacon, C. A., Brandsdóttir, B., Eibl, E. P. S., Glastonbury-Southern, E., Gudnason, E. Á., Hersir, G. P. & Horálek, J. (2022). Deep long period seismicity preceding and during the

2021 Fagradalsfjall eruption, Iceland. *Bulletin of Volcanology* **84**, 1–20. https://doi.org/10.1007/s00445-022-01603-2.

Grove, T. L., Kinzler, R. J. & Bryan, W. B. (1992). Fractionation of mid-ocean ridge basalt (MORB). *Gephysical Monograph-American Geophysical Union* **71**, 281–310. https://doi.org/10.1029/GM071p0281.

Gunnarson, S. R., Belart, J. M. C., Óskarsson, B. V., Gudmundsson, M. T., Högnadóttir, T., Pedersen, G. B. M., Dürig, T. & Pinel, V. (2023). Automated processing of aerial imagery for geohazards monitoring: results from Fagradalsfjall eruption, SW Iceland, august 2022. Zenodo.

Halldórsson, S. A., Bali, E., Hartley, M. E., Neave, D. A., Peate, D. W., Guðfinnsson, G. H., Bindeman, I., Whitehouse, M. J., Riishuus, M. S., Pedersen, G. B. M., Jakobsson, S., Askew, R., Gallagher, C. R., Guðmundsdóttir, E. R., Gudnason, J., Moreland, W. M., Óskarsson, B. V., Nikkola, P., Reynolds, H. I., Schmith, J. & Thordarson, T. (2018). Petrology and geochemistry of the 2014–2015 Holuhraun eruption, Central Iceland: compositional and mineralogical characteristics, temporal variability and magma storage. *Contributions to Mineralogy and Petrology* **173**, 1–25. https://doi.org/10.1007/s00410-018-1487-9.

Halldórsson, S. A., Marshall, E. W., Caracciolo, A., Matthews, S., Bali, E., Rasmussen, M. B., Ranta, E., Robin, J. G., Guðfinnsson, G. H., Sigmarsson, O., Maclennan, J., Jackson, M. G., Whitehouse, M. J., Jeon, H., van der Meer, Q. H. A., Mibei, G. K., Kalliokoski, M. H., Repczynska, M. M., Rúnarsdóttir, R. H., Sigurðsson, G., Pfeffer, M. A., Scott, S. W., Kjartansdóttir, R., Kleine, B. I., Oppenheimer, C., Aiuppa, A., Ilyinskaya, E., Bitetto, M., Giudice, G. & Stefánsson, A. (2022). Rapid shifting of a deep magmatic source at Fagradalsfjall volcano, Iceland. *Nature* **609**, 529–534. https://doi.org/10.1038/s41586-022-04981-x.

Hanks, T. C. & Kanamori, H. (1979). A moment magnitude scale. *Journal of Geophysical Research* **84**, 2348–2350. https://doi.org/10.1029/JB084iB05p02348.

Higgins, O., & Stock, M. J. (2024). A New Calibration of the OPAM Thermobarometer for Anhydrous and Hydrous Mafic Systems. *Journal of Petrology*, **65**(5). https://doi.org/10.1093/petrology/egae043.

Hjartardóttir, Á. R., Dürig, T., Parks, M., Drouin, V., Eyjólfsson, V., Gies, N., Pedersen, G. B. M. & Einarsson, P. (2023). Eruptive vent openings during the 2021 Fagradalsfjall eruption, Iceland, and their relationship with pre-existing fractures. *Bulletin of Volcanology* **85**, 10330. https://doi.org/10.1007/s00445-023-01670-z.

Holzapfel, C., Chakraborty, S., Rubie, D. C. & Frost, D. J. (2007). Effect of pressure on Fe–Mg, Ni and Mn diffusion in (FexMg1-x)2SiO4olivine. *Physics of the Earth and Planetary Interiors* **162**, 186–198. https://doi.org/10.1016/j.pepi.2007.04.009.

Iacovino, K. & Till, C. B. (2019). DensityX: a program for calculating the densities of magmatic liquids up to 1,627 °C and 30 kbar. *VOLCANICA* **2**, 1–10. https://doi.org/10.30909/vol.02.01.0110.

Jenkins, J., Greenfield, T., White, R. S., Maclennan, J., Gudnason, E. Á., Ágústsdóttir, T., Rawlinson, N., Obermann, A., Dahm, T., Milkereit, C., Rahimi Dalkhani, A., Fone, J., Hersir, G. P. & Doubravova, J. (2025). Seismic imaging of the Reykjanes Peninsula, Iceland: crustal-scale context of geothermal areas and ongoing volcano-tectonic unrest. *Geochemistry, Geophysics, Geosystems* **26**. https://doi.org/10.1029/2024GC011817.

Kahl, M., Chakraborty, S., Pompilio, M. & Costa, F. (2015). Constraints on the nature and evolution of the magma plumbing system of Mt. Etna volcano (1991-2008) from a combined thermodynamic and kinetic modelling of the compositional record of minerals. *Journal of Petrology* **56**, 2025–2068. https://doi.org/10.1093/petrology/egv063.

Kahl, M., Mutch, E. J. F., Maclennan, J., Morgan, D. J., Couperthwaite, F., Bali, E., Thordarson, T., Guðfinnsson, G. H., Walshaw, R., Buisman, I., Buhre, S., van der Meer, Caracciolo, A., Marshall, E. W., Rasmussen, M. B., Gallagher, C. R., Moreland, W. M., Höskuldsson, Á. & Askew, R. A. (2023). Deep magma mobilization years before the 2021 CE Fagradalsfjall eruption, Iceland. *Geology* **51**, 184–188. https://doi.org/10.1130/G50340.1.

Krättli, G. & Schmidt, M. W. (2021). Experimental settling, floatation and compaction of plagioclase in basaltic melt and a revision of melt density. *Contributions to Mineralogy and Petrology* **176**. https://doi.org/10.1007/s00410-021-01785-6.

Kress, V. C. & Carmichael, I. S. E. (1991). The compressibility of silicate liquids containing Fe2O3 and the effect of composition, temperature, oxygen fugacity and pressure on their redox states. *Contributions to Mineralogy and Petrology* **108**, 82–92. https://doi.org/10.1007/BF00307328.

Lamb, O. D., Gestrich, J. E., Barnie, T. D., Ducrocq, C., Shore, M. J., Lees, J. M. & Lee, S. J. (2021). Acoustic observations of lava fountain activity during the 2021 Fagradalsfjall eruption, Iceland. *Bulletin of Volcanology* **84**, 1–18. https://doi.org/10.1007/s00445-022-01602-3.

Lo Forte, F. M., Aiuppa, A., Rotolo, S. G. & Zanon, V. (2023). Temporal evolution of the Fogo Volcano magma storage system (Cape Verde Archipelago): a fluid inclusions perspective. *Journal of Volcanology and Geothermal Research* **433**, 107730. https://doi.org/10.1016/j.jvolgeores.2022.107730.

Maclennan, J. (2019). Mafic tiers and transient mushes: evidence from Iceland. *Philosophical Transactions of the Royal Society A* **377**, 20180021–20180020. https://doi.org/10.1098/rsta.2018.0021.

Magee, C., Stevenson, C. T. E., Ebmeier, S. K., Keir, D., Hammond, J. O. S., Gottsmann, J. H., Whaler, K. A., Schofield, N., Jackson, C. A. L., Petronis, M. S., O'Driscoll, B., Morgan, J., Cruden, A., Vollgger, S. A., Dering, G., Micklethwaite, S. & Jackson, M. D. (2018). Magma plumbing systems: a geophysical perspective. *Journal of Petrology* **59**, 1217–1251. https://doi.org/10.1093/petrology/egy064.

Mann, H. B. & Whitney, D. R. (1947). On a test of whether one of two random variables is stochastically larger than the other. *The Annals of Mathematical Statistics* **18**, 50–60. https://doi.org/10.1214/aoms/1177730491.

Marshall, E. W., Caracciolo, A., Bali, E., Halldórsson, S. A., Matthews, S., Ranta, E., Rasmussen, M. B., Robin, J. G., Guðfinnson, G. H., Maclennan, J., Bosq, C., Auclair, D., Sigmarsson, O., Merrill, H., Gísladóttir, B., Johnson, S., Löw, N., Stracke, A. & Genske, F. (2024). The petrology and geochemistry of the 2021 Fagradalsfjall eruption, Iceland: an eruption sourced from multiple, compositionally diverse, near-Moho sills. *AGU Advances* **5**, e2024AV001310. https://doi.org/10.1029/2024AV001310.

Matthews, S. W., Caracciolo, A., Bali, E., Halldórsson, S. A., Sigmarsson, O., Guðfinnsson, G. H., Pedersen, G. B. M., Robin, J. G., Marshall, E. W., Aden, A. A., Gísladóttir, B. Ý., Bosq, C., Auclair, D., Merrill, H., Levillayer, N., Löw, N., Rúnarsdóttir, R. H., Johnson, S. M., Steinþórsson, S. & Drouin, V. (2024). A dynamic mid-crustal magma domain revealed by the 2023 to 2024 Sundhnúksgígar eruptions, Iceland. *Science* **386**, 309–314. https://doi.org/10.1126/science.adp8778.

Meissner, R. & Strehlau, J. (1982). Limits of stresses in continental crusts and their relation to the depth-frequency distribution of shallow earthquakes. *Tectonics* **1**, 73–89. https://doi.org/10.1029/TC001i001p00073.

Moore, A., Coogan, L. A., Costa, F. & Perfit, M. R. (2014). Primitive melt replenishment and crystal-mush disaggregation in the weeks preceding the 2005-2006 eruption 9°50' N, EPR. *Earth and Planetary Science Letters* **403**, 15–26. https://doi.org/10.1016/j.epsl.2014.06.015.

Mutch, E. J. F., Maclennan, J., Holland, T. J. B. & Buisman, I. (2019a). Millennial storage of near-Moho magma. *Science* **365**, 260–264. https://doi.org/10.1126/science.aax4092.

Mutch, E. J. F., Maclennan, J., Shorttle, O., Edmonds, M. & Rudge, J. F. (2019b). Rapid transcrustal magma movement under Iceland. *Nature Geoscience* **12**, 569–574. https://doi.org/10.1038/s41561-019-0376-9.

Mutch, E. J. F., Maclennan, J., Shorttle, O., Rudge, J. F. & Neave, D. A. (2021). DFENS: diffusion chronometry using finite elements and nested sampling. *Geochemistry, Geophysics, Geosystems* **22**, 1–28. https://doi.org/10.1029/2020GC009303.

Mutch, E. J. F., Maclennan, J. & Madden-Nadeau, A. L. (2022). The dichotomous nature of Mg partitioning between plagioclase and melt: implications for diffusion chronometry. *Geochimica et Cosmochimica Acta* **339**, 173–189. https://doi.org/10.1016/j.gca.2022.10.035.

Namur, O., Charlier, B., Toplis, M. J., & Vander Auwera, J. (2011). Prediction of plagioclase-melt equilibria in anhydrous silicate melts at 1-atm. *Contributions to Mineralogy and Petrology*, **163**(1), 133–150. https://doi.org/10.1007/s00410-011-0662-z.

Neave, D. A., Bali, E., Guðfinnsson, G. H., Halldórsson, S. A., Kahl, M., Schmidt, A.-S., & Holtz, F. (2019). Clinopyroxene–Liquid Equilibria and Geothermobarometry in Natural and Experimental Tholeiites: the 2014–2015 Holuhraun Eruption, Iceland. *Journal of Petrology*, **60**(8), 1653–1680. https://doi.org/10.1093/petrology/egz042.

Neave, D. A. & Namur, O. (2022). Plagioclase archives of depleted melts in the oceanic crust. *Geology* **50**, 848–852. https://doi.org/10.1130/G49840.1.

Neave, D. A. & Putirka, K. D. (2017). A new clinopyroxene-liquid barometer, and implications for magma storage pressures under Icelandic rift zones. *American Mineralogist* **102**, 777–794. https://doi.org/10.2138/am-2017-5968.

Parks, M., Sigmundsson, F., Drouin, V., Hjartardóttir, Á. R., Geirsson, H., Hooper, A., Vogfjörd, K. S., Ófeigsson, B. G., Hreinsdóttir, S., Jensen, E. H., Einarsson, P., Barsotti, S. & Fridriksdóttir, H. M. (2023). Deformation, seismicity, and monitoring response preceding and during the 2022 Fagradalsfjall eruption, Iceland. *Bulletin of Volcanology* **85**, 1–16. https://doi.org/10.1007/s00445-023-01671-y.

Parks, M., Drouin, V., Sigmundsson, F., Hjartardóttir, Á. R., Geirsson, H., Pedersen, G. B. M., Belart, J. M. C., Barsotti, S., Lanzi, C., Vogfjörd, K., Hooper, A., Ófeigsson, B., Hreinsdóttir, S., Gestsson, E. B., Þrastarson, R. H., Einarsson, P., Tolpekin, V., Rotheram-Clarke, D., Gunnarsson, S. R., Óskarsson, B. V. & Pinel, V. (2025). 2023–2024 inflation-deflation cycles at Svartsengi and repeated dike injections and eruptions at the Sundhnúkur crater row, Reykjanes Peninsula, Iceland. *Earth and Planetary Science Letters* **658**, 119324. https://doi.org/10.1016/j.epsl.2025.119324.

Peate, D. W., Baker, J. A., Jakobsson, S. P., Waight, T. E., Kent, A. J. R., Grassineau, N. V. & Skovgaard, A. C. (2009). Historic magmatism on the Reykjanes Peninsula, Iceland: a snap-shot of melt generation at a ridge segment. *Contributions to Mineralogy and Petrology* **157**, 359–382. https://doi.org/10.1007/s00410-008-0339-4.

Pedersen, G. B. M., Belart, J. M. C., Óskarsson, B. V., Gudmundsson, M. T., Gies, N., Högnadóttir, T., Hjartardóttir, Á. R., Pinel, V., Berthier, E., Dürig, T., Reynolds, H. I., Hamilton, C. W., Valsson, G., Einarsson, P., Ben-Yehosua, D., Gunnarsson, A. & Oddsson, B. (2022). Volume, effusion rate, and lava transport during the 2021 Fagradalsfjall eruption: results from near real-time photogrammetric monitoring. *Geophysical Research Letters* **49**, 1–11. https://doi.org/10.1029/2021GL097125.

Pedersen, G. B. M., Belart, J. M. C., Óskarsson, B. V., Gunnarson, S. R., Gudmundsson, M. T., Reynolds, H. I., Valsson, G., Högnadóttir, T., Pinel, V., Parks, M. M., Drouin, V., Askew, R. A., Dürig, T. & Drastarson, R. H. (2024) *Volume, effusion rates and lava hazards of the 2021, 2022 and 2023 Reykjanes fires: Lessons learned from near real-time photogrammetric monitoring*. EGU General Assembly 2024, Vienna, Austria, 14–19 Apr 2024, EGU24-10724, https://doi.org/10.5194/egusphere-egu24-10724, 2024.

Petry, C., Chakraborty, S. & Palme, H. (2004). Experimental determination of Ni diffusion coefficients in olivine and their dependence on temperature, composition, oxygen fugacity, and crystallographic orientation. *Geochimica et Cosmochimica Acta* **68**, 4179–4188. https://doi.org/10.1016/j.gca.2004.02.024.

Putirka, K. D. (2008). Thermometers and barometers for volcanic systems. *Reviews in Mineralogy and Geochemistry* **69**, 61–120. https://doi.org/10.2138/rmg.2008.69.3.

Roeder, P. L. & Emslie, R. F. (1970). Olivine–liquid equilibrium. *Contribution to MIneralogy and Petrology* **29**, 275–289. https://doi.org/10.1007/BF00371276.

Rooyakkers, S. M., Carroll, K. J., Gutai, A. F., Winpenny, B., Bali, E., Guðfinnsson, G. H., Maclennan, J., Sigmundsson, F., Jónasson, K., Mutch, E. J. F., Neave, D. A., Robin, J. G., Grönvold, K. & Halldórsson, S. A. (2024). Hydraulically linked reservoirs simultaneously fed the 1975–1984 Krafla Fires eruptions: insights from petrochemistry. *Earth and Planetary Science Letters* **646**, 118960. https://doi.org/10.1016/j.epsl.2024.118960.

Sæmundsson, K., Sigurgeirsson, M. A., Hjartarson, Á., Kaldal, I. & Kristinsson, S. G. (2016) *Geological Map of Southwest Iceland, 1: 100 000*, 2nd edn. Reykjavik: Iceland GeoSurvey.

Sæmundsson, K., Sigurgeirsson, M. & Friðleifsson, G. Ó. (2020). Geology and structure of the Reykjanes volcanic system, Iceland. *Journal of Volcanology and Geothermal Research* **391**, 106501. https://doi.org/10.1016/j.jvolgeores.2018.11.022.

Scott, D. W. (2010). Scott's rule. *Wiley Interdisciplinary Reviews: Computational Statistics* **2**, 497–502. https://doi.org/10.1002/wics.103.

Scott, S. W., Pfeffer, M., Oppenheimer, C., Bali, E., Lamb, O. D., Barnie, T., Woods, A. W., Kjartansdóttir, R. & Stefánsson, A. (2023). Near-surface magma flow instability drives cyclic lava fountaining at Fagradalsfjall, Iceland. *Nature Communications* **14**, 1–9. https://doi.org/10.1038/s41467-023-42569-9.

Shorttle, O. & Maclennan, J. (2011). Compositional trends of Icelandic basalts: implications for short-length scale lithological heterogeneity in mantle plumes. *Geochemistry, Geophysics, Geosystems* **12**, 1–32. https://doi.org/10.1029/2011GC003748.

Sigmarsson, O., Condomines, M., Gronvold, K. & Thordarson, T. (1991). Extreme magma homogeneity in the 1783-84 Lakagigar eruption: origin of a large volume of evolved basalt in Iceland. *Geophysical Research Letters* **18**, 2229–2232. https://doi.org/10.1029/91GL02328.

Sigmundsson, F., Parks, M., Hooper, A., Geirsson, H., Vogfjörd, K. S., Drouin, V., Ófeigsson, B. G., Hreinsdóttir, S., Hjaltadóttir, S., Jónsdóttir, K., Einarsson, P., Barsotti, S., Horálek, J. & Ágústsdóttir, T. (2022). Deformation and seismicity decline before the 2021 Fagradalsfjall eruption. *Nature Cell Biology* **609**, 523–528. https://doi.org/10.1038/s41586-022-05083-4.

Sigmundsson, F., Parks, M., Geirsson, H., Hooper, A., Drouin, V., Vogfjörd, K. S., Ófeigsson, B. G., Greiner, S. H. M., Yang, Y., Lanzi, C., de Pascale, G. P., Jónsdóttir, K., Hreinsdóttir, S., Tolpekin, V., Friðriksdóttir, H. M., Einarsson, P. & Barsotti, S. (2024). Fracturing and tectonic stress drive ultrarapid magma flow into dikes. *Science* **383**, 1228–1235. https://doi.org/10.1126/science.adn2838.

Soubestre, J., Caudron, C., Melnik, O., Lecocq, T., Jaupart, C., Shapiro, N. M., Journeau, C., Çubuk-Sabuncu, Y. & Jónsdóttir, K. (2025). Dynamics of the 2021 Fagradalsfjall eruption (Iceland) revealed by volcanic tremor patterns. *Journal of Geophysical Research: Solid Earth*. John Wiley and Sons Inc **130**. https://doi.org/10.1029/2024JB029380.

Spandler, C. & O'Neill, H. S. C. (2010). Diffusion and partition coefficients of minor and trace elements in San Carlos olivine at 1,300°C with some geochemical implications. *Contributions to Mineralogy and Petrology* **159**, 791–818. https://doi.org/10.1007/s00410-009-0456-8.

Wadge, G. (1981). The variation of magma discharge during basaltic eruptions. *Journal of Volcanology and Geothermal Research* **11**, 139–168. https://doi.org/10.1016/0377-0273(81)90020-2.

Wieser, P. E., Petrelli, M., Lubbers, J., Wieser, E., Özaydın, S., Kent, A. J. R. & Till, C. B. (2022). Thermobar: an open-source Python3 tool for thermobarometry and hygrometry. *Volcanica* **5**, 349–384. https://doi.org/10.30909/vol.05.02.349384.

Zellmer, G. F. (2021). Gaining acuity on crystal terminology in volcanic rocks. *Bulletin of Volcanology* **83**. https://doi.org/10.1007/s00445-021-01505-9.

Journal of Petrology, 2025, **66**, egaf054
https://doi.org/10.1093/petrology/egaf054
Original Manuscript